Article

SOURCE DATA | TRANSPARENT PROCESS | OPEN ACCESS

THE EMBO JOURNAL

TOR acts as a metabolic gatekeeper for auxin-dependent lateral root initiation in *Arabidopsis thaliana*

Michael Stitz[1], David Kuster[1], Maximilian Reinert[1], Mikhail Schepetilnikov[2], Béatrice Berthet[1], Jazmin Reyes-Hernández[1], Denis Janocha[1], Anthony Artins[3], Marc Boix[4], Rossana Henriques[5], Anne Pfeiffer[1], Jan Lohmann[1], Emmanuel Gaquerel[2,*] & Alexis Maizel[1,**]

Abstract

Plant organogenesis requires matching the available metabolic resources to developmental programs. In *Arabidopsis*, the root system is determined by primary root-derived lateral roots (LRs), and adventitious roots (ARs) formed from non-root organs. Lateral root formation entails the auxin-dependent activation of transcription factors ARF7, ARF19, and LBD16. Adventitious root formation relies on LBD16 activation by auxin and WOX11. The allocation of shoot-derived sugar to the roots influences branching, but how its availability is sensed for LRs formation remains unknown. We combine metabolic profiling with cell-specific interference to show that LRs switch to glycolysis and consume carbohydrates. The target-of-rapamycin (TOR) kinase is activated in the lateral root domain. Interfering with TOR kinase blocks LR initiation while promoting AR formation. The target-of-rapamycin inhibition marginally affects the auxin-induced transcriptional response of the pericycle but attenuates the translation of ARF19, ARF7, and LBD16. TOR inhibition induces WOX11 transcription in these cells, yet no root branching occurs as TOR controls LBD16 translation. TOR is a central gatekeeper for root branching that integrates local auxin-dependent pathways with systemic metabolic signals, modulating the translation of auxin-induced genes.

Keywords *Arabidopsis thaliana*; auxin; lateral root; metabolism; TOR
Subject Categories Plant Biology
DOI 10.15252/embj.2022111273 | Received 25 March 2022 | Revised 27 February 2023 | Accepted 3 March 2023 | Published online 6 April 2023
The EMBO Journal (2023) 42: e111273

Introduction

Plants assimilate atmospheric CO_2 in their leaves and convert it into simple sugars by photosynthesis. Sucrose is the predominant sugar transported from the source tissues to heterotrophic sink tissues, where it is hydrolyzed to fructose and glucose that fuels growth and development.

The root system fulfills essential functions, and its architecture is postembryonically determined by lateral roots (LRs), which originate from the growing primary root, and adventitious roots (ARs), which are formed from stems or leaf tissues in response to environmental and physiological stresses (Bellini *et al*, 2014). The root system is an obligate sink organ, and mounting evidence suggests that allocating sugars to roots drives primary root growth and lateral root development, two main determinants of the root system architecture. Shortly after germination, light triggers root growth via the transport of photosynthesis-derived sugar into the root tip (Kircher & Schopfer, 2012), and increased photosynthetic rates in aboveground tissues correlate with increased LR formation (Crookshanks *et al*, 1998). Crosstalk between carbon metabolism and phytohormone signaling, mainly auxin signaling, has been linked to the modulation of root system architecture (Sairanen *et al*, 2012). Regardless of the known role sugar plays in LR development, our knowledge about how sugars and glucose modulate LR formation at the molecular level remains unknown.

Lateral root formation is an auxin-controlled process. In *Arabidopsis thaliana* (hereafter *Arabidopsis*), it occurs through the activation of pericycle cells facing the xylem pole that become founder cells and undergo a series of cell divisions to form a primordium that emerges from the primary root (Malamy & Benfey, 1997). The earliest marker of LR initiation is their radial swelling, repolarization, and nuclei migration toward the common anticlinal wall (Schütz *et al*, 2021). Additional founder cells are recruited (Torres-Martínez

1 Center for Organismal Studies, Heidelberg University, Heidelberg, Germany
2 Institut de Biologie Moleculaire des Plantes (IBMP), UPR CNRS 2357, Strasbourg, France
3 Max Planck Institute of Molecular Plant Physiology, Potsdam, Germany
4 Centre for Research in Agricultural Genomics, Barcelona, Spain
5 Environmental Research Institute, University College Cork, Cork, Ireland
*Corresponding author. Tel: +33 3 67 15 53 52; E-mail: emmanuel.gaquerel@ibmp-cnrs.unistra.fr
**Corresponding author. Tel: +49 6221 54 64 56; E-mail: alexis.maizel@cos.uni-heidelberg.de

© 2023 The Authors. Published under the terms of the CC BY NC ND 4.0 license

et al, 2020), which further proliferate and form a dome-shaped LR primordium (LRP) (Lucas *et al*, 2013). Upregulation of auxin signaling (Dubrovsky *et al*, 2008) and *GATA23* expression (De Rybel *et al*, 2010) are two molecular markers associated with LR founder cells and initiation. Auxin-dependent gene regulation plays a major role in all stages of LR development. It occurs through TRANSPORT INHIBITOR RESISTANT 1/AUXIN SIGNALING F-BOX (TIR1/AFB) induced degradation of the AUXIN/INDOLEACETIC ACID (Aux/IAA) repressors that frees the transcriptional activators AUXIN RESPONSE FACTORS (ARFs) inducing expression of downstream genes (Blázquez *et al*, 2020). During LR initiation, Aux/IAA 14 (*IAA14*, *SOLITARY ROOT*), *ARF7*, and *ARF19* are necessary for cell cycle entry (Fukaki *et al*, 2002) and activation of LATERAL ORGAN BOUNDARY (LBD) 16, a transcription factor, is required for the asymmetric division of these cells (Okushima *et al*, 2007). LR and AR have similar mechanisms for primordium development but are triggered by divergent initial processes (Bellini *et al*, 2014). WUSCHEL-RELATED HOMEOBOX11 (WOX11) is required to initiate ARs from hypocotyl and activates *LBD16* (Sheng *et al*, 2017). While WOX11 is not involved in LR initiation when plants are vertically grown on medium, the primary root can produce both WOX11-mediated roots and ARF7/19-mediated LRs when plants are grown in soil or upon wounding (Sheng *et al*, 2017). This noncanonical WOX11-mediated primary root branching (also called "adventitious lateral root,"; Ge *et al*, 2019) contributes to the plasticity of the Arabidopsis root system architecture. The cell and mechanistic bases of lateral root and adventitious root initiation start to be elucidated (Atkinson *et al*, 2014; Santos Teixeira & Ten Tusscher, 2019). However, insight into how the plant's metabolic status is integrated into regulating this developmental program is mostly unknown.

Energy availability perception is mediated in plants by two evolutionarily conserved and counteracting kinases (Shi *et al*, 2018). The SUCROSE NONFERMENTING1-RELATED PROTEIN KINASE1 (SnRK1) promotes catabolic metabolism, contrasting the TARGET OF RAPAMYCIN (TOR) kinase that promotes anabolic, energy-consuming processes. TOR forms a complex (TORC) consisting of TOR and the TOR-interacting proteins RAPTOR (regulatory-associated protein of mTOR, RAPTOR1A, and RAPTOR1B) and LST8 (small lethal with SEC13 protein 8, LST8-1, and LST8-2) (Menand *et al*, 2002; Moreau *et al*, 2012). While *tor*-null mutants are embryonic lethal (Menand *et al*, 2002), the predominantly expressed regulatory proteins RAPTOR1B and LST8-1 show viable mutant phenotypes (Salem *et al*, 2017). TORC is activated by nutrients (Dobrenel *et al*, 2016) such as glucose and branched-chain amino acids (Cao *et al*, 2019) as well as phytohormones such as auxin (Schepetilnikov *et al*, 2017). It phosphorylates targets linked to the cell cycle, translation, lipid synthesis, N assimilation, autophagy, and ABA signaling (Shi *et al*, 2018). The usage of inducible TOR knockdown lines (Xiong *et al*, 2013) and specific chemical inhibitors such as AZD8055 (Montané & Menand, 2013) led to the discovery of a mechanistic connection between TOR and its phosphorylation substrates to a multitude of developmental processes (Van Leene *et al*, 2019). In particular, TOR is essential for activating the embryo-derived root and shoot meristems during the photoautotrophic transition (Xiong *et al*, 2013). While TOR plays a central role in coordinating the energy status of plants with several developmental programs from embryo development to senescence (Shi *et al*, 2018), it remains unknown whether TOR plays a role in the postembryonic establishment of new meristems like in the case of LR formation. Two reports suggest a possible link between energy availability sensing pathways and LR formation. Using an engineered rapamycin-sensitive version of TOR in potato, it was shown that TOR is necessary for hypocotyl-borne (adventitious) root formation (Deng *et al*, 2017) and, recently, SnRK1 was shown to be required for LR formation induced by unexpected darkness (Muralidhara *et al*, 2021).

Here, we examine the role of TOR in LR formation and its interplay with auxin signaling. Using a combination of root metabolomics profiling, sugar metabolism manipulation, chemical/genetic and tissue-specific inhibition of TOR-dependent signaling, and genome-wide profiling of TOR effects on transcriptome and translatome, we present evidence that TOR activation in the LR founder cells and subsequent LR initiation are coordinated by high glycolysis rates depending on shoot-derived sugar. We further show that TOR inhibition marginally affects the auxin-induced transcriptional response of the pericycle but attenuates the translation of ARF19, ARF7, and LBD16. TOR inhibition also induces the AR program by inducing WOX11 transcription, yet as it simultaneously attenuates the translation of LBD16, no primary root branching occurs. These data place TOR as a central gatekeeper for postembryonic root branching that integrates local auxin-dependent pathways with systemic metabolic signals, modulating the translation of auxin-induced gene expression.

Results and Discussion

Plants with impaired lateral root formation hyperaccumulate starch in foliage

Lateral root formation is an energy-demanding process that depends on shoot-derived carbon. Photoassimilates not consumed immediately by the plant's foliar metabolism are stored as transitory starch granules and consumed in the dark until the onset of the light period (Graf *et al*, 2010). We first set out to assess how LR carbon demand impacts foliar carbon metabolism by performing starch staining in seedlings impaired in different steps of the auxin signaling cascade, specifically controlling LR formation (Fig 1A). At the end of the dark period, starch accumulation was limited in wild-type Col-0 seedlings, indicated by the characteristic purple stain (Fig 1B). Globally, impairing auxin signaling in LR-less *iaa14/solitary root* (*slr*) and *arf7/arf19* mutant plants resulted in dark purple coloration throughout the leaves, indicative of higher levels of starch accumulation (Fig 1B). ARF7 and ARF19 are regulators for the transcriptional activation of *LBD16*, and plants expressing a dominant repressor version of LBD16 (*LBD16-SRDX*) do not form LR (Goh *et al*, 2012). Starch staining in LR-less *LBD16-SRDX* seedlings led to comparably intense dark coloration as observed for *slr* foliage, indicating that blocking LR formation by interfering with the auxin signaling cascade or its direct targets leads to hyperaccumulation of photoassimilates in leaves. Notably, starch accumulation in *arf7/arf19* was less pronounced. To ascertain that this increased accumulation of starch was caused by the lack of LRs and not a systemic effect of interfering with auxin signaling, we performed starch staining in *pGATA23::shy2-2-GR* and *pGATA23::slr1-GR* plants. These lines express dominant repressor versions of *SLR* and *SHY2/IAA3*,

 © 2023 The Authors

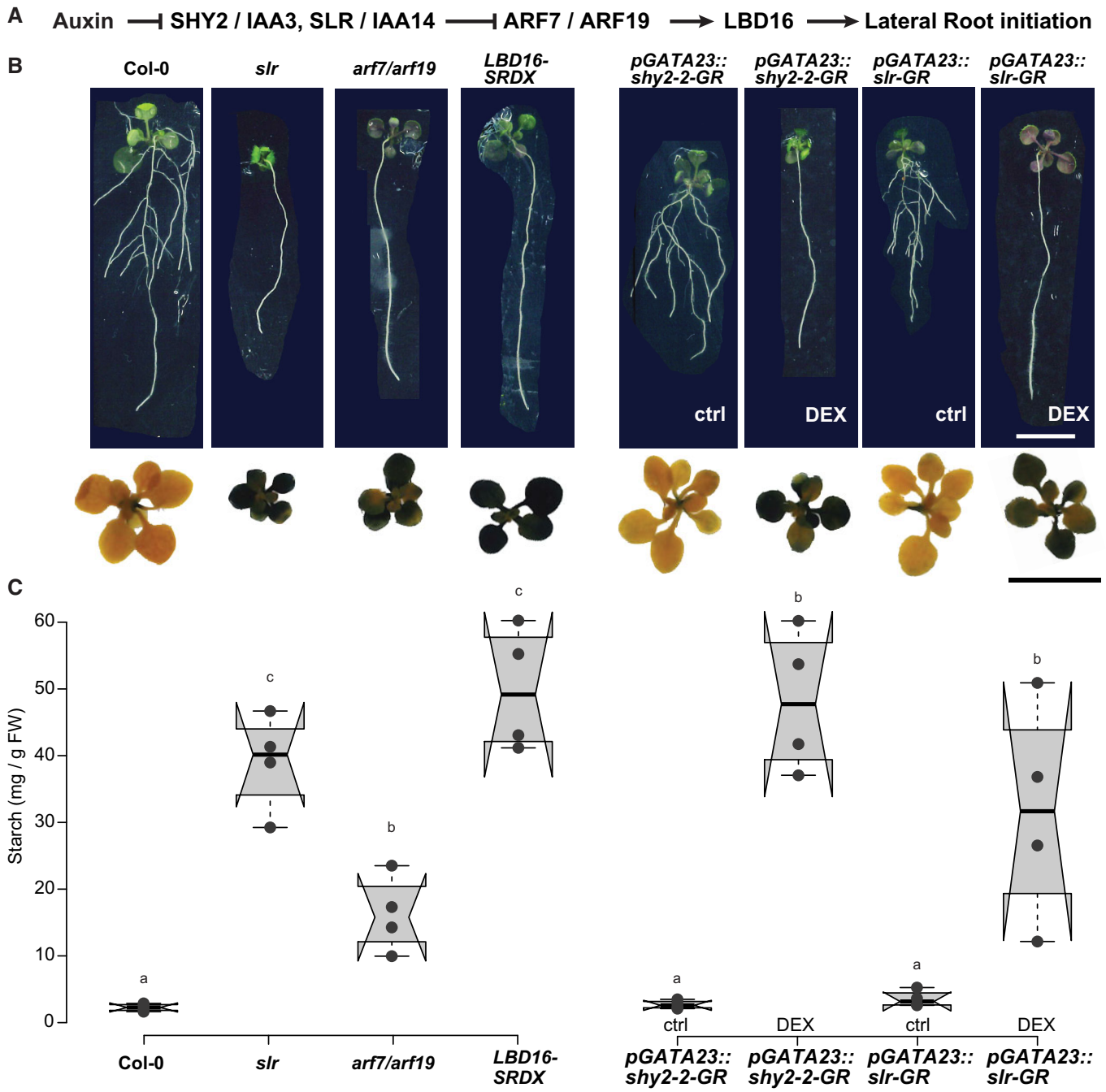

Figure 1. Lateral root deficiency leads to starch hyperaccumulation in leaves.

A Schematic representation of key components of the auxin signaling module acting during lateral root initiation.

B Images of rosettes and seedlings (15 DAG) of Col-0, *arf7/arf19*, *slr*, and *gLBD16-SRDX* as well as the inducible lateral-root-less lines *pGATA23::shy2-2-GR* and *pGATA23::slr1-GR* grown on DMSO control medium or 30 μM Dexamethasone (DEX), Scale bar 1 cm. The rosettes were stained with a Lugol's Iodine solution for starch accumulation at the end of the dark period (representative images of $n = 3$ biological replicates).

C Box plots of starch quantification in rosette tissues at 15 DAG ($n = 4$ biological replicates). Comparison between samples was performed by one-way ANOVA and *post-hoc* Tukey HSD Test ($\alpha = 0.05$); different letters indicate significant differences.

Source data are available online for this figure.

specifically in the pericycle upon application of dexamethasone (DEX), resulting in an inducible, pericycle-specific inhibition of auxin signaling and LR formation (Ramakrishna *et al*, 2019). Whereas control-treated lines showed faint purple coloration in leaves comparable with that in Col-0 plants, upon DEX treatment, we observed intense starch accumulation in the leaves, indicating

© 2023 The Authors

that, similar to the global effect observed in the *slr*, *arf7/19* and *gLBD16-SRDX* mutants, blocking LR formation specifically in the root pericycle is sufficient to induce starch hyperaccumulation in foliage (Fig 1B). This hyperaccumulation of starch in LR-less genotypes can be observed as early as 12 DAG (Appendix Fig S1). We did not observe any differences in foliar starch accumulation between these genotypes at the end of the light period, indicating that these plants do not differ in their ability to accumulate starch but to consume starch during the dark period (Appendix Fig S2). We quantified starch abundance to assess the differences in starch accumulation in more detail (Fig 1C). The elevated starch levels in LR-less genotypes confirmed the observations of the starch staining. Notably, starch accumulation is less pronounced in the *arf7/arf19* double mutant compared with the other LR-less mutants. This observation might be attributed to other regulatory factors of the primary metabolism in leaves that might not be affected in *arf7/arf19*—possibly other ARFs downstream of *SLR*—that may contribute to the sink strength of the root. Taken together, these observations point toward LR formation and its associated resource consumption to drive an increase in demand for shoot-derived carbon sources, in agreement with starch being a major integrator of plant growth regulation (Sulpice *et al*, 2009).

Auxin-triggered pericycle activation depends on shoot-derived carbohydrate catabolism in the root

To monitor changes in central carbon pathways resulting from the metabolism of shoot-derived carbohydrates and associated with the formation of LR, we conducted nontargeted metabolomics by gas chromatography coupled with mass spectrometry from shoot and root samples collected after synchronous activation of the pericycle (Himanen *et al*, 2002). Briefly, after a pretreatment with the auxin transport inhibitor NPA (N-1-naphthylphthalamic acid, 10 μM for 24 h) that prevents pericycle activation, 7-day-old seedlings were shifted to a medium containing auxin (Indole-3-acetic acid, IAA 10 μM) to activate the entire pericycle synchronously. This induction system allows the synchronization of the pericycle and recapitulates the onset of the lateral root initiation program (Vanneste *et al*, 2005; Lavenus *et al*, 2013; Ramakrishna *et al*, 2019; Vilches Barro *et al*, 2019; Ursache *et al*, 2021). By activating the entire pericycle, we circumvent that at any given time, only a few cells are activated, and the analysis of the metabolites would be dominated by the nonactivated cells. Shoot and root samples were dissected and collected at six time points (0, 2, 6, 12, 24, and 30 h) after transferring seedlings from NPA to IAA to induce LR formation or maintaining them on NPA as control (Fig 2A). This time series covers LR formation from pericycle activation to stage V. By applying this procedure to wild-type (Col-0) and *slr* mutant seedlings in which pericycle activation is prevented (Vanneste *et al*, 2005), we aimed to infer a metabolic signature associated specifically with the activation of the pericycle marking LR initiation. To this end, raw metabolomics data were deconvoluted to extract compound-derived mass spectra used for annotation and statistical analysis. From a pool of more than 400 deconvoluted spectra, we conducted a hierarchical clustering analysis of the top 250 ones that exhibited nonconstant intensity levels across the genotype x treatment x time matrix (Fig 2B; Dataset EV1). This clustering analysis revealed that IAA induced several phases of reconfigurations of the root carbon metabolism in Col-0, which were largely altered in the *slr* mutant. Most specifically, cluster #1 comprised IAA-responsive compounds that were characterized in Col-0 roots by a slow build-up rate (reaching maximum values at 30 h post-IAA); the latter response was mostly impaired in the *slr* mutant (Fig 2B). Cluster #2 and a subpart cluster #4 were characterized by IAA-responsive compounds, which reached much greater relative levels in the *slr* mutant 12 h after transfer to IAA than in Col-0 roots (Fig 2B).

We next mined clusters for metabolites associated with these IAA−/*slr*-dependent root metabolome responses. In line with the starch staining data, glucose and sucrose levels were slightly higher in *slr* shoot tissues than in Col-0 (Appendix Fig S3). Upon shift to IAA, levels of shoot sucrose quickly increased within 2 h, and while they kept increasing for up to 12 h in *slr*, it plateaued in WT. This and the starch hyperaccumulation in shoots upon LR impairment indicate that LR formation relies on a sucrose transfer from the shoot. In seedlings, photosynthetically derived sucrose has been described as an interorgan signal and fuel to drive the primary root growth (Kircher & Schopfer, 2012). For up to 24 h after shifting to IAA, sucrose levels built up similarly in root tissues of both Col-0 and *slr* and then became significantly higher in Col-0 than *slr* (Fig 2C), in line with a weaker sink strength of *slr* resulting from its inability to form LRs. From the clustering, we looked at the levels of added sugars and glycolytic intermediates found to be deregulated in *slr* roots (Fig 2B and C). The root levels of glucose and fructose derived from sucrose cleavage increased for 6 h upon IAA in Col-0 and then decreased until the end of the night period. Noticeably, glucose and fructose levels were strongly increased by the IAA treatment in the *slr* mutant and peaked at 12 h (Fig 2C). This suggests that upon pericycle activation, glucose and fructose derived from sucrose cleavage do not build up, probably due to their catabolism by glycolysis, the latter being reduced in the absence of pericycle activation (*slr* mutant). A similar IAA-dependent overaccumulation was detected for several additional sugars enriched within the IAA-regulated cluster visible at 12 h in *slr* (Fig 2B), such as the disaccharide trehalose, the polyol *myo*-inositol as well as glucose-6-P and fructose-6-P. Notably, glucose-6-P is produced by the hexokinase1 (HXK1), which, when mutated, was reported to reduce LR formation (Gupta *et al*, 2015) supporting that Glucose-6-P levels are instrumental for LR formation, a notion further supported in a recent study that showed that WOX7, a WUSCHEL-related transcription factor, acts downstream of HXK1 to regulate LR formation (Li *et al*, 2020). The accumulation of glucose-6-P and fructose-6-P, two glycolysis intermediates, was in contrast with their normally low steady-state abundance (e.g., in Col-0 NPA/IAA conditions) characteristic of their rapid consumption by the glycolytic flux (Arrivault *et al*, 2009). Interestingly, soluble carbohydrates have been demonstrated to promote auxin biosynthesis (Sairanen *et al*, 2012). The accumulation of carbohydrates in roots when LR formation is compromised could thus explain the previously reported elevated levels of auxin observed in *slr* mutants (Vanneste *et al*, 2005). Downstream in the carbohydrate catabolic pathway, the prolonged increases in the levels of several intermediates of the tricarboxylic acid (TCA), observed in Col-0 but not in *slr*, indicate that auxin-induced LR formation increases the catabolic flux. Levels of several amino acids whose biosynthetic pathways connect to the TCA cycle further indicated that an upregulation of energy-releasing and amino

 © 2023 The Authors

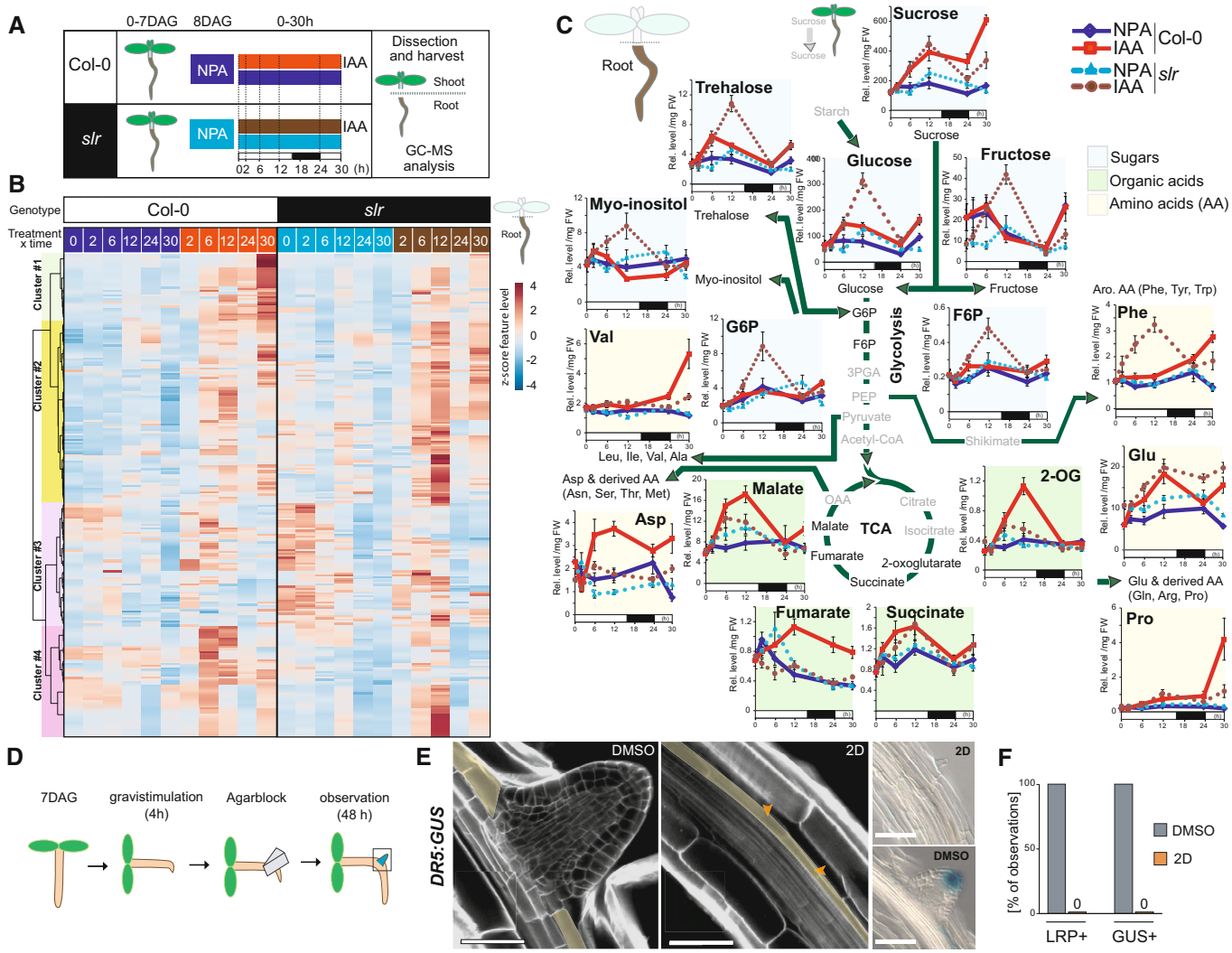

Figure 2. Increased flux within sugar glycolytic catabolism and connected pathways precede and are essential for LR formation.

A Schematic of the experimental setup used for the GC–MS-based metabolomics profiling.

B Heatmap from a hierarchical clustering analysis (HCA) with Ward's linkage showing z-score normalized relative levels of top 250 most intense compound-derived spectra (Dataset EV1) exhibiting non-constant intensity (One-way ANOVA & FDR-adjusted $P < 0.05$) across experimental conditions in roots. Main HCA clusters are color labeled.

C Mean relative levels (± SE, $n = 5$ biological replicates, normalized to the ribitol internal standard and per mg fresh weight) for representative metabolites of sugar, glycolytic, tricarboxylic acid, amino acid metabolic pathways in root tissues of Col-0 (solid lines) and *slr* (dashed lines) at the indicated time after IAA application. The white and black boxes below the *x*-axis indicate light and dark phases during the sampling. Statistical differences for genotype × treatment (NPA- vs. IAA-treated roots) are summarized in Dataset EV1.

D Schematic of the experimental setup for induction of LR formation upon local 2-deoxy-D-glucose (2D, 10 mM) treatment.

E Representative confocal sections of calcofluor counterstained (E, $n = 5$ biological replicates) and differential interference contrast (DIC) images of GUS-stained root bends (F, $n = 16$ biological replicates) in *DR5:GUS* seedlings treated as indicated 48 h after gravistimulation. In (E), orange arrows indicate the pericycle (marked in yellow). Scale bar: 50 µm.

F Fraction of root bends forming an LRP and showing DR5 GUS staining after treatment with either control or 2D containing agar blocks ($n = 16$ biological replicates, ± SE).

Source data are available online for this figure.

acid production pathways, previously reported at the transcriptomic level (Dembinsky *et al*, 2007; Appendix Fig S4) and here backed up by metabolite data, underpins early stages of LR formation and is impaired in *slr*. Together these data indicate that the auxin-induced pericycle activation and re-entry in division are associated with a switch to glycolysis. This observation echoes similar ones in animals where the acquisition of pluripotency has been linked to a switch to glycolysis, supporting the concept of metabolic reprogramming of cell fate (Shyh-Chang & Ng, 2017).

To verify whether this activation of sugar usage through glycolysis is indeed required for LR initiation and to rule out an effect of exogenous auxin, we induced LR initiation by gravistimulation (Lavenus *et al*, 2015) in the presence of 2-deoxy-d-glucose (2D) a nonmetabolizable glucose analog blocking glycolysis. 2D was

© 2023 The Authors

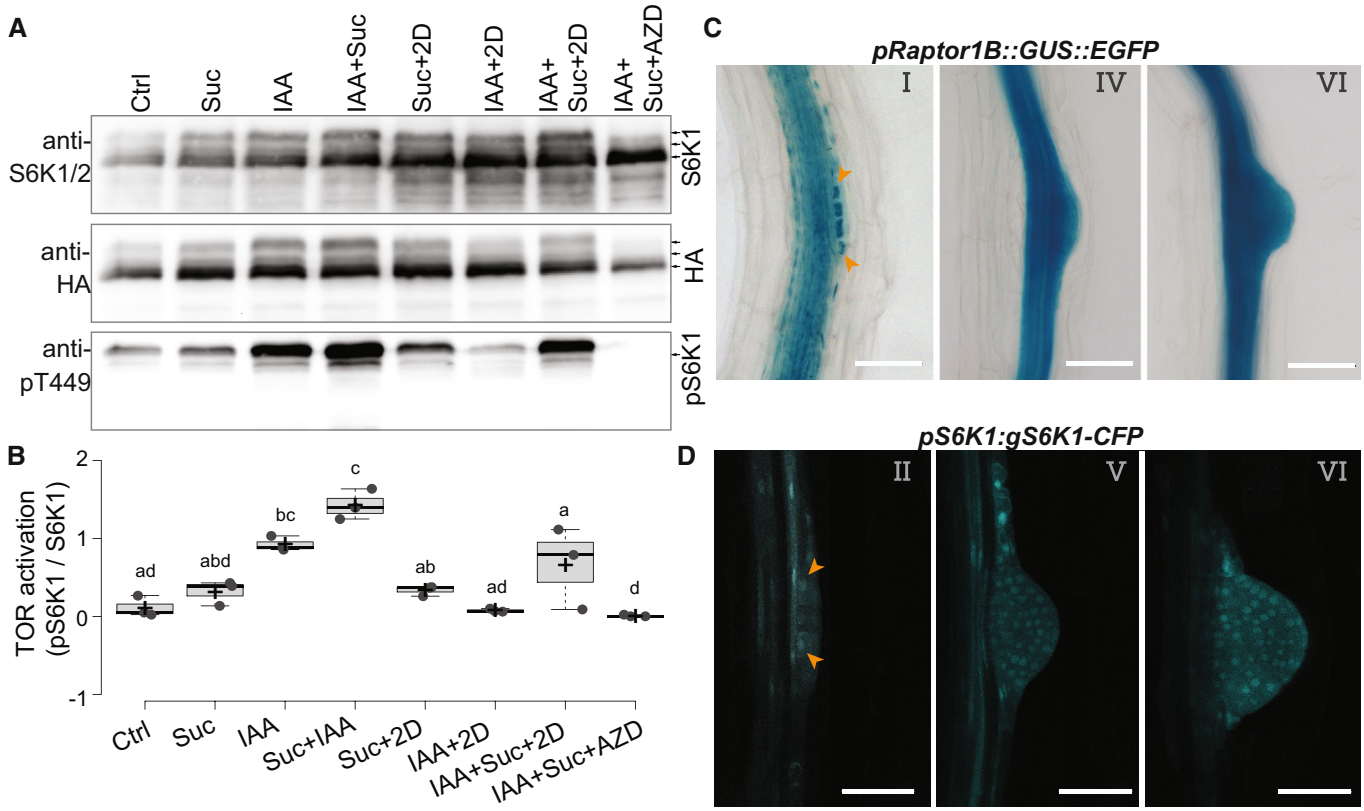

Figure 3. Auxin inducible S6K1 phosphorylation via TOR depends on the activation of glycolysis in the primary root.

A Representative western blot of root tissues of *pUB10:S6K1-3xHA* treated by the indicated combination of auxin (IAA, 10 μM), sucrose (Suc, 110 mM), 2-deoxy-d-glucose (2D, 20 mM) and AZD8055 (AZD, 10 μM) and probed with anti-S6K1/2, anti-HA or anti-S6K1-T449P. Blot is one of three biological replicates.

B Quantification of the relative S6K activation. Box plots show three biological replicates, and comparison between samples was performed by one-way ANOVA and *post-hoc* Tukey HSD Test ($\alpha = 0.05$); different letters indicate significant differences.

C Representative DIC images showing *RPT1B* promoter expression at different stages of LR development in 10 DAG seedlings. Orange arrowheads indicate the accumulation of reporter signals in the dividing lateral root founder cells. Scale bars: 50 μm.

D Representative confocal section showing S6K1 expression in different stages of LR development in 10 DAG *pS6K1:gS6K1-CFP* seedlings. Orange arrowheads indicate the accumulation of reporter signals in the dividing lateral root founder cells. Scale bars: 50 μm.

Source data are available online for this figure.

applied locally by an agar block positioned over the root bend (Fig 2D). Whereas in mock-treated root bends, an LR primordium developed, none were formed upon 2DG treatment where the pericycle cells facing the xylem pole showed no divisions (Fig 2E and F). Auxin accumulation in the pericycle acts as a morphogenetic trigger for LR formation and is one of the earliest markers of LR initiation (Dubrovsky *et al*, 2008). To monitor auxin accumulation upon glycolysis inhibition, we stained root bends treated with 2DG for *DR5:GUS*. We did not detect DR5 activity in the bend upon 2DG treatment (Fig 2E and F). These indicate that inhibition of glycolysis blocks LR initiation at a very early stage.

Together these data show that glycolysis and glycolysis-dependent metabolic activations are required to form an LR.

The TOR complex is activated upon lateral root induction

Lateral root formation is an auxin-induced process regulated by glucose (Gupta *et al*, 2015) and requires carbohydrate catabolism (our results). The TOR complex (TORC) is required for shoot and root meristems activation (Xiong *et al*, 2013; Pfeiffer *et al*, 2016; Li *et al*, 2017) and is activated by glucose in shoots and roots (Xiong *et al*, 2013; Pfeiffer *et al*, 2016; Li *et al*, 2017) and additionally by auxin in the shoot (Xiong *et al*, 2013; Li *et al*, 2017; Schepetilnikov *et al*, 2017), we hypothesized that re-activation of cell proliferation during LR induction could lead to TORC activation. We monitored the phosphorylation of the canonical TORC substrate S6K1 in roots upon treatment with sucrose and IAA (Fig 3A and B). Treatment with either sucrose or IAA led to an upregulation of S6K1 phosphorylation, while co-treatment had a synergistic effect that was fully suppressed by treatment with the TORC inhibitor AZD8055 (Montané & Menand, 2013). Treating roots with IAA led to a glycolytic switch (Fig 2B and C); thus, we sought to check to which extent IAA's effects on TORC activation depend on glycolysis. For this, we repeated the sucrose and IAA treatments in the presence of 2D. Simultaneous provision of external 2D and sucrose did not lower the levels of pS6K1, possibly due to an excess of sucrose. Inhibition of glycolysis without additional sucrose led to a block of S6K1 phosphorylation induced by IAA, indicating that TORC activation by

 © 2023 The Authors

auxin depends on carbohydrate catabolism in roots. This glycolysis-dependent promotion of TOR activity by auxin could be a specificity of heterotrophic tissues that allows a systemic integration of developmental progression with shoot photosynthetic capacity. Such coupling has been reported for the light-dependent regulation of alternative splicing in roots triggered by shoot-photosynthesized sugars and compromised when TOR levels or its activity is reduced (Riegler *et al*, 2021).

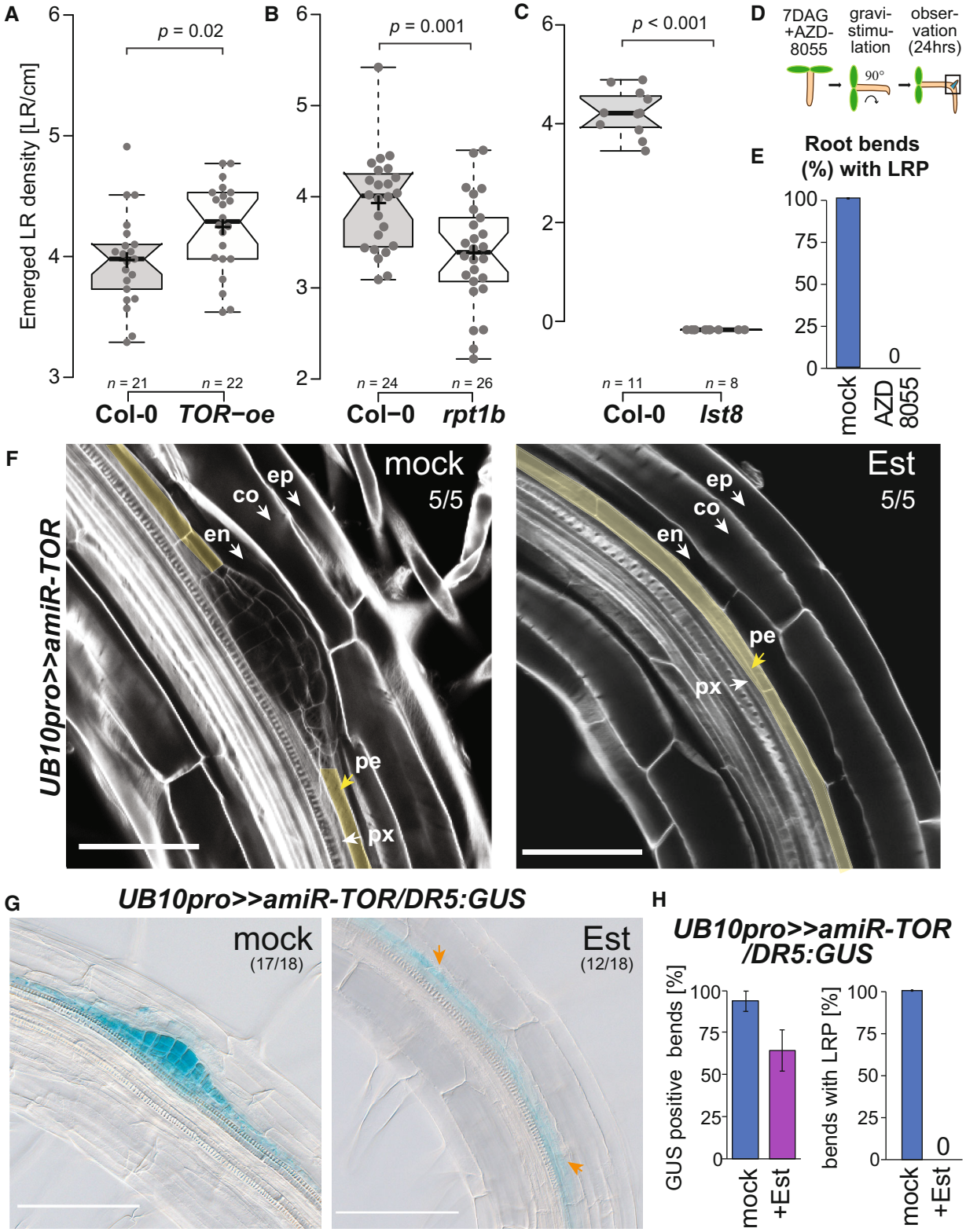

Figure 4.

Figure 4. TORC is required in the pericycle for lateral root formation.

A–C Box plots of emerged LR in *TOR-oe* (A), *rpt1b* (B), and *lst8* (C) at 14 DAG. Comparison between samples was performed by one-way ANOVA and *post-hoc* Tukey HSD Test ($\alpha = 0.05$); different letters indicate significant differences. The number of roots scored is indicated.

D Schematic of the experimental setup used for scoring LR formation by gravistimulation upon inhibition of TOR by AZD8055 (10 μM).

E Proportion of bends developing lateral root primordia after transfer to AZD8055 containing media and gravistimulation for 24 h ($n = 10$).

F Representative confocal images of calcofluor counterstained bends of 7DAG *UB10pro>>amiR-TOR* seedlings following a 24 h pre-treatment with mock (DMSO) or ß-Estradiol (10 μM) and subsequent 24 h gravistimulation (ep: epidermis, co: cortex, en: endodermis, pe: pericycle, px: protoxylem). Numbers indicate the proportion of root bends with the depicted phenotype. Scale bar: 50 μm.

G Representative DIC images of bends in 7 DAG *UB10pro>>amiR-TOR/DR5:GUS* seedlings stained for GUS activity after a 24 h pre-treatment with mock (DMSO) or ß-Estradiol (Est, 10 μM) and subsequent 24 h gravistimulation. The proportion of root bends showing the depicted phenotype is indicated. Scale bar: 100 μm.

H Fraction of bends developing lateral root primordia and stained for GUS activity in primary root vasculature of *UB10pro>>amiR-TOR/DR5:GUS*, $n = 18$ bends.

Source data are available online for this figure.

The previous results do not identify in which cells TOR is activated. To pinpoint in which tissues the TORC is present and active, we first used a reporter for the TORC subunit RAPTOR1B and detected its expression in the stele, LR founder cells of the pericycle, and LR primordia (Fig 3C). This expression pattern is similar to the one reported for the other TORC subunit LST8 (Moreau *et al*, 2012). It suggests that TORC is present in the stele, the activated pericycle, founder cells, and forming LR. We also monitored in which cells S6K1 is expressed using a CFP-tagged genomic clone. This reporter specifically marked the actively dividing LR founder cells (Fig 3D), confirming an earlier report (Zhang *et al*, 1994). These results suggest that TORC is turned on in the activated pericycle cells but do not exclude that it could also be activated in the stele tissue important for pericycle activation, such as the protoxylem.

The TOR complex is required for LR formation

The glucose-TOR signaling and the phytohormone jasmonate were recently shown to determine the branching angle of LR (Sharma *et al*, 2022). We looked at LR formation in plants with altered TORC levels or activity to test whether TORC is necessary for forming LR. We first used a *TOR* overexpression line (*TOR-oe*; Deprost *et al*, 2007) and observed longer primary roots and increased density of emerged LR, indicating that elevated TOR levels can promote LR formation (Fig 4A; Appendix Fig S5). *TOR*-null mutants are embryo-arrested (Menand *et al*, 2002); we thus first quantified LR density in *raptor1b* (*rpt1b*) and *lst8*, two viable mutants that lead to reduced TOR activity (Moreau *et al*, 2012; Salem *et al*, 2017). Lateral root density was reduced in *rpt1b* and *lst8*, indicating that the full TORC activity might be necessary for proper LR formation (Fig 4B and C; Appendix Fig S5). Notably, the development of hypocotyl-born adventitious roots was increased in the *lst8* mutant (Fig EV1). To further confirm that TORC activity is required for LR formation, we treated wild-type seedlings with AZD8055 (AZD). Lateral root initiation occurs in a region of the root where the endodermal Casparian stripe severely limits the apoplastic diffusion (Vermeer *et al*, 2014); we thus had to treat seedlings with 10 μM AZD, a concentration that fully inhibits primary root growth (Montané & Menand, 2013). To circumvent this shortcoming and be able to monitor the effect of TORC inhibition on LR formation, we turned to gravistimulation-induced LR formation (Fig 4D, Lavenus *et al*, 2015). In these conditions, AZD treatment led to a complete block of LR formation (Fig 4E). To test the contribution of *TOR* itself to LR formation, we designed a ß-estradiol (Est) inducible artificial miRNA against *TOR* that we first expressed from the *UBIQUITIN* promoter (*UB10pro>>amiR-TOR*). After 24 h of Est treatment, *TOR* mRNA abundance was reduced to < 25% of that of the DMSO control indicating efficient knockdown of *TOR* mRNA (Appendix Fig S6). When LR formation was induced by gravistimulation in these conditions, we did not observe any division of the pericycle in the bend. At the same time, we observed stage III LR primordia in DMSO-treated plants (Fig 4F). Notably, we observed that upon TOR knockdown, while LR formation was inhibited, AR formation from the hypocotyl was not (Fig EV1). Together, these data indicate that chemical and genetic inhibition of TOR kinase leads to a block of LR initiation and promotes AR formation in the hypocotyl.

As an exogenous application of sugar or auxin can promote LR formation and increase TOR activity, we checked whether the block in LR formation induced by knocking down *TOR* could be reversed by treatments with auxin and/or sucrose. Neither sole nor combined applications of sucrose or auxin could rescue the inhibition of LR formation induced by the *TOR* knockdown (Appendix Fig S7). Reducing the abundance or activity of TOR blocks LR formation early, indicating an essential role for TOR. To determine whether *TOR* was required, particularly in the LR founder cells, we knocked down *TOR* in the xylem pole pericycle (XPP) cells from which LR founder cells derive (Parizot *et al*, 2008). For this, we drove the expression of the amiR-TOR from the XPP-specific promoter (Andersen *et al*, 2018) using a dexamethasone (Dex) inducible expression system (*XPPpro>>amiR-TOR*). Impaired TORC function leads to starch accumulation in foliage (Caldana *et al*, 2013). We observed that Est-treated *UB10pro>>amiR-TOR* hyperaccumulated starch in their leaves (Appendix Fig S8). Similarly, we observed intense starch accumulation around the leaf vasculature in DEX-treated *XPPpro>>amiR-TOR*, suggesting TOR knockdown (Appendix Fig S8). In the root, induction of *amiR-TOR* in the XPP cells led to a severe reduction in the number and density of emerged LR formed compared with mock-induced plants (Fig EV2A and B). However, induction of LR by gravistimulation did not impair initiation events (Fig EV2C and D). Given that the promoter driving the expression of the amiR-TOR switches off as soon as LR initiation starts (Andersen *et al*, 2018), this indicates that sustained downregulation of TOR is required in the pericycle to suppress the initiation of LR formation. The severe reduction in the number and density of emerged LR may be a consequence of the re-activation of the *XPPpro>>amiR-TOR* in the newly formed LR primordium.

To determine whether auxin accumulation was compromised in the *TOR* knockdown, we crossed the *pDR5::GUS* to the *UB10pro>>amiR-TOR* line. In control conditions, we observed *pDR5::GUS* accumulation in the apical region of the stage III

 © 2023 The Authors

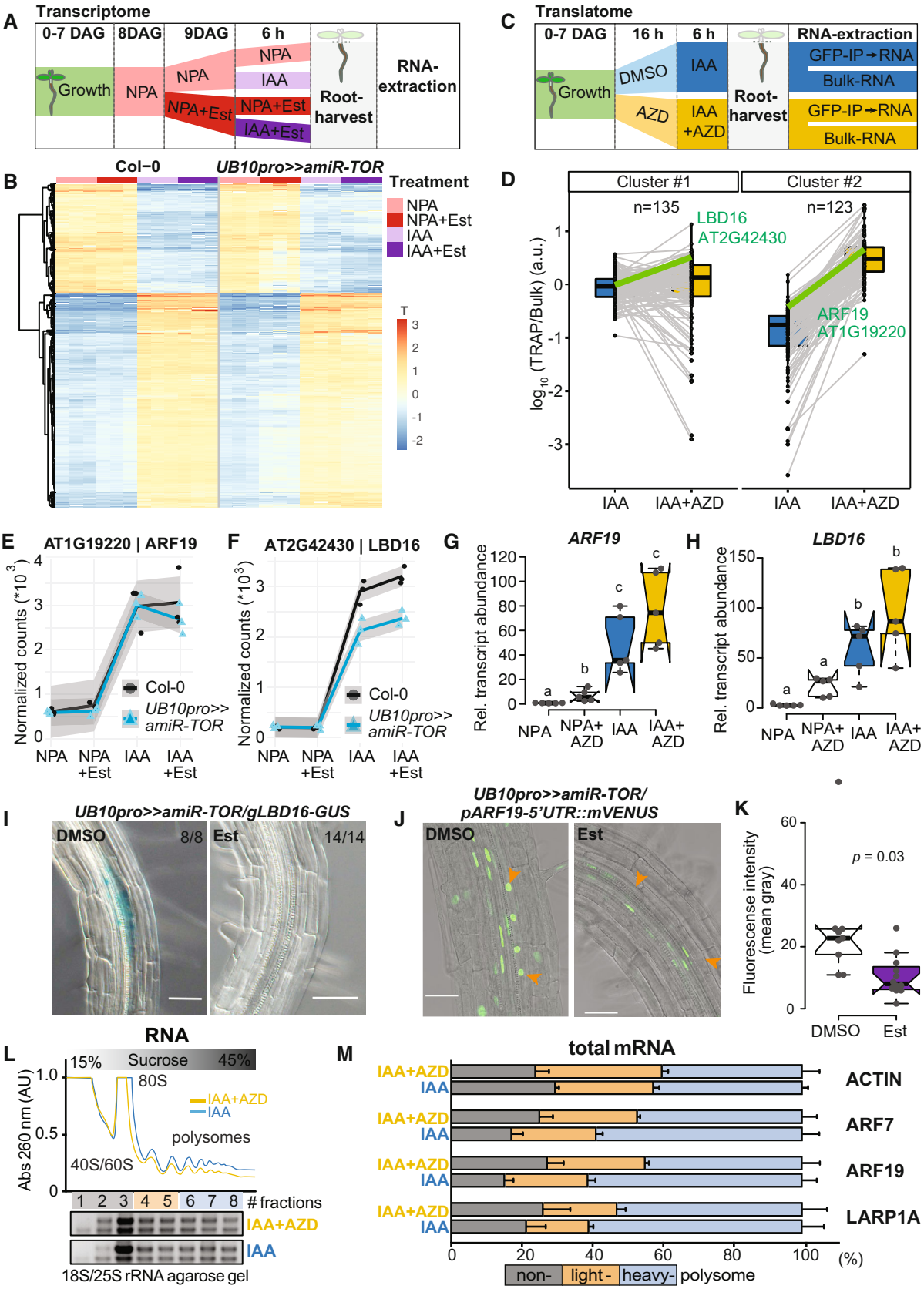
A
Transcriptome
0-7 DAG
8DAG
9DAG
6 h
Growth
NPA
NPA
NPA+Est
NPA
IAA
NPA+Est
IAA+Est
Root-harvest
RNA-extraction
C
Translatome
0-7 DAG
16 h
6 h
RNA-extraction
Growth
DMSO
AZD
IAA
IAA +AZD
Root-harvest
GFP-IP→RNA
Bulk-RNA
GFP-IP→RNA
Bulk-RNA
B
Col−0
UB10pro>>amiR-TOR
Treatment
NPA
NPA+Est
IAA
IAA+Est
T
3
2
1
0
-1
-2
D
Cluster #1
Cluster #2
n=135
n=123
LBD16
AT2G42430
ARF19
AT1G19220
log10 (TRAP/Bulk) (a.u.)
1
0
-1
-2
-3
IAA
IAA+AZD
IAA
IAA+AZD
E
AT1G19220 | ARF19
Normalized counts (*10^3)
4
3
2
1
0
Col-0
UB10pro>> amiR-TOR
NPA
NPA +Est
IAA
IAA +Est
F
AT2G42430 | LBD16
Normalized counts (*10^3)
3
2
1
0
Col-0
UB10pro>> amiR-TOR
NPA
NPA +Est
IAA
IAA +Est
G
ARF19
Rel. transcript abundance
120
100
80
60
40
20
0
a
b
c
c
NPA
NPA+ AZD
IAA
IAA+ AZD
H
LBD16
Rel. transcript abundance
150
100
50
0
a
a
b
b
NPA
NPA+ AZD
IAA
IAA+ AZD
I
UB10pro>>amiR-TOR/gLBD16-GUS
DMSO
8/8
Est
14/14
J
UB10pro>>amiR-TOR/ pARF19-5'UTR::mVENUS
DMSO
Est
K
Fluorescense intensity (mean gray)
60
40
20
0
p = 0.03
DMSO
Est
L
RNA
15%
Sucrose
45%
Abs 260 nm (AU)
1.0
0.5
0
80S
IAA+AZD
IAA
polysomes
40S/60S
1 2 3 4 5 6 7 8 # fractions
IAA+AZD
IAA
18S/25S rRNA agarose gel
M
total mRNA
IAA+AZD
IAA
ACTIN
ARF7
ARF19
LARP1A
0
20
40
60
80
100
(%)
non-
light -
heavy-
polysome

Figure 5.

Figure 5. Effect of TOR on the auxin-induced lateral root transcriptome and translatome.

A Schematic of the experimental setup used to profile the impact of *TOR* knockdown on the transcriptome during LR formation. IAA, NPA, and Est were all used at 10 μM concentration.

B Heatmap from a k-means clustering analysis for 1,141 IAA-dependent transcripts (log fold change > 1 & FDR < 0.05). $n = 3$ biological replicates.

C Schematic of the experimental setup used to profile the impact of *TOR* inhibition on the translatome during LR formation. IAA and AZD8055 were used at 10 μM.

D Translational response (reads associated to ribosomes (TRAP) divided by reads in Bulk RNA) of 258 auxin-induced genes. K-means revealed two clusters, with mild (#1) to strong (#2) shifts in translation response upon TOR inhibition. The profiles of *ARF19* and *LBD16* are highlighted in green. $n = 3$ biological replicates.

E, F Abundance of *ARF19* (E) and *LBD16* (F) transcripts in RNAseq samples. mRNA accumulation in response to auxin is comparable for both, whether TOR is knocked down. $n = 3$ biological replicates.

G, H Relative expression levels (normalized to *ACTIN*) of *ARF19* (G) and *LBD16* (H) measured by RT–qPCR upon TOR activity inhibition with AZD8055. Comparison between samples was performed by one-way ANOVA. Different letters indicate significant differences based on a *post-hoc* Tukey HSD Test ($n = 5$ biological replicates, $\alpha = 0.05$).

I Distribution of GUS-staining in *UB10pro>>amiR-TOR/gLBD16-GUS* seedlings 24 h after bending is absent if previously treated for 24 with Est. The proportion of root bends with the depicted phenotype is indicated.

J Representative confocal images of bends of 7 DAG *UB10pro>>amiR- TOR/pARF19-5′UTR::mVENUS* seedlings following a 24 h pre-treatment with mock (DMSO) or ß-Estradiol and subsequent 24 h gravistimulation. Scale bar: 50 μm, $n = 9$ root bends.

K Signal (mean gray values) in the nuclei of the pericycle cells of *UB10pro>>amiR-TOR/pARF19-5′UTR::mVENUS*. Significant differences between DMSO and Est-treated roots based on paired *t*-test, $n = 9$ root bends.

L, M Total lysates prepared from lateral roots treated or not with IAA and AZD were fractionated through sucrose gradients, and the relative redistribution (percentage of total) of *ACTIN*, *ARF7*, *ARF19*, and *LARP1* mRNAs in every 8 fractions were studied by RT–qPCR analysis. (L) Polysome profiles. 40S, small ribosomal subunit; 60S, large ribosomal subunit; 80S, mono-ribosome; polysomes, polyribosomes. AU is arbitrary units of RNA absorbance at A260 nanometers. (M) RT–qPCR analysis of mRNA redistribution through a sucrose gradient (8 fractions collected). Translation efficiency was computed as a percentage of mRNA in non-polysome fractions (40/60/80S; fractions 1–3) against both lights (fractions 4–5) and heavy polysomes (fractions 6–8). The plot is representative of three independently performed experiments with similar results. Data are mean ± SEM.

Source data are available online for this figure.

LR-primordia 24 h after gravistimulation. Upon *TOR* knockdown, we detect in ~ 60% of the LR a faint DR5::GUS signal in the pericycle and the protoxylem (Fig 4G and H). Collectively, these data suggest that while *TOR* is required for LR initiation, TOR knockdown does not cause complete inhibition of auxin signaling.

TOR inhibition moderately affects the transcriptional auxin response associated with LR formation

While the reduction of *TOR* abundance or inhibition of its activity blocks LR formation, it does not fully block auxin signaling in these cells, suggesting that it is required either downstream or parallel to the auxin-induced LR formation developmental program. To obtain a genome-wide picture of the effects of *TOR* knockdown during the early phase of LR formation, we compared by RNA-seq the transcriptomes of roots 6 h after the auxin-induced synchronous pericycle activation (Himanen *et al*, 2002) in the inducible *UB10pro>>amiR-TOR* background (Fig 5A). Transcriptome analysis identified 1,141 auxin-responsive genes in control conditions (Appendix Fig S9). Upon *TOR* knockdown, the expression of these genes was barely changed (Fig 5B). We verified that inhibition of TOR activity by treatment with AZD8055 led to similar effects (Appendix Fig S10). Although no morphological sign of LR initiation in the pericycle could be observed upon *TOR* knockdown or inhibition, the auxin-induced transcriptional response was globally unchanged. The SLR/IAA14 protein is a central regulator of LR initiation that controls the auxin-dependent expression of genes in the pericycle essential for LR initiation (Fukaki *et al*, 2002). We thus examined in detail how this set of IAA-induced genes behaved upon *TOR* knockdown. For this, we took advantage of an existing dataset that profiles the response of the pericycle in similar conditions upon inhibition of *SLR*-dependent auxin signaling in the pericycle (Ramakrishna *et al*, 2019) and identified 475 SLR-dependent genes responsive to auxin. These genes behaved the same in *TOR* knockdown and controls, indicating that although LR formation is inhibited, the transcriptional SLR-dependent response to auxin in the pericycle is globally unaffected when *TOR* levels are reduced. Together these data suggest that upon *TOR* reduction, founder cells still perceive and respond transcriptionally to auxin but appear unable to transform this response into an LR initiation event.

TOR affects the translation of auxin-responsive transcription factors

The contrast between the mild effect of *TOR* knockdown on the root transcriptome and the strong block of LR formation prompted us to investigate the effects of TOR inhibition on the translatome. To this end, we performed targeted purification of polysomal mRNA (TRAP-Seq; Vragović *et al*, 2015) using a transgenic line ubiquitously expressing a GFP-tagged RPL18 (Mustroph *et al*, 2009) 6 h after the synchronous pericycle activation by auxin treatment upon inhibition of TOR activity (AZD8055 treatment, AZD). To correct for the abundance of mRNA, bulk RNA-Seq was performed on the same samples and used to normalize the reads purified with the ribosomes (Fig 5C). This TRAP/Bulk ratio measures the fraction of mRNA associated with ribosomes, be it polysomes or monosomes, and provides an indication of the degree of translation of a particular mRNA. The bulk RNA-seq data analysis identified 271 transcripts upregulated upon IAA treatment. Although this number is reduced compared with the transcriptome analysis due to the absence of NPA pretreatment, 80% of these genes were also differentially expressed in the *UB10pro>>amiR-TOR* transcriptome upon IAA treatment (Appendix Fig S11). Clustering these transcripts according to their TRAP/Bulk ratio between IAA and IAA + AZD conditions revealed two clusters. Cluster #1 consists of genes with moderate change in TRAP/Bulk ratio comparing IAA to IAA + AZD, whereas the change was more important for cluster #2 (Fig 5D). Examining these two clusters, we selected two candidates for further

 © 2023 The Authors

characterization, LBD16 (cluster #1) and ARF19 (cluster #2), both involved in LR initiation (Okushima *et al*, 2007).

In the *UB10pro>>amiR-TOR* transcriptome, these two genes were induced by IAA, and this induction was not affected by knocking down *TOR* (Fig 5E and F). This result was independently confirmed by RT–qPCR upon inhibition of TOR activity by AZD8055 (Fig 5G and H), indicating that transcription of these genes is not affected by TOR abundance or activity. In the translatome data, both genes had a higher TRAP/Bulk ratio upon inhibition of TOR activity. This suggests that the translation of these genes is different when TOR is inhibited. To verify this, we crossed the *UB10pro>>amiR-TOR* line to translational reporters for ARF19 and LBD16 and monitored the effect of *TOR* knockdown on the expression of the reporters. For ARF19, the expression of the mVenus reporter is controlled by the ARF19 promoter, the 5′UTR, and the 1st intron (*pARF19-5′UTR::mVenus*; Truskina *et al*, 2021). For LBD16, we used a GUS-tagged genomic clone (Sheng *et al*, 2017). In both cases, whereas in control conditions, expression of the reporters could be detected in the cells of the LR primordium, upon *TOR* knockdown, their translation was severely reduced while still present in the neighboring cells (Fig 5I–K). This indicates that TOR controls the expression of these two genes during LR initiation at the translational level. Similar results for ARF19 accumulation were obtained in roots following synchronized LR-induction via auxin treatment, confirming the comparability of gravitropic induction (single LR) and proliferation of numerous LRs using the lateral root inducible system (Fig EV3). To further confirm that TOR can regulate the expression of genes at the translation level, we looked at the association of the endogenous ARF19 transcript with ribosomes in wild-type plants treated or not with AZD8055 during auxin-induced LR formation. Comparing the polysome profile upon TOR inhibition to the control revealed a shift from heavy to light fractions indicative of a reduced ribosome processivity (Fig 5L and M). This shift was comparable with the one observed for *LARP1*, a transcript whose translation is TOR-dependent (Scarpin *et al*, 2020). Note that the distribution among ribosomal fractions was similar under both conditions for the housekeeping gene *ACTIN* (Fig 5M). As ARF19 and ARF7 are jointly essential for LR initiation (Okushima *et al*, 2007), we also profiled the association of *ARF7* mRNA, whose expression is not auxin-induced, with ribosomes. Like *ARF19*, *ARF7* mRNA shifted from heavy to light fractions upon TOR inhibition, indicating that its translation is controlled by TOR (Fig 5M). Together these data show that the translation of both key transcription factors mediating auxin signaling during LR initiation is modulated by TOR. Intriguingly, the 5′UTR of both *ARF7* and *ARF19* mRNA contains several upstream open reading frames (uORF) that require a TOR-dependent translation re-initiation step to allow expression of the main ORF (Schepetilnikov *et al*, 2013), providing a likely mechanism by which TOR could regulate the expression of these genes. Collectively, our data support a model in which TOR acts as a metabolic gatekeeper for LR formation by locally integrating the availability of shoot-derived photoassimilates with the auxin-mediated LR developmental program through control of the translation of key transcription factors. Such a model would ensure the integration and coordination of the developmental and metabolic cues required to form a new organ. Given the vast array of TOR outputs, it is likely that TOR may exert its gatekeeper role through additional mechanisms, such as promoting cell cycle progression via E2F as previously established (Xiong *et al*, 2013).

TOR inhibits WOX11 expression in the root and controls noncanonical primary root branching

Given that ARF7 and ARF19 regulate the transcriptional activation of LBD16, and TOR controls their translation, we wondered how *LBD16* transcripts still accumulate upon TOR inhibition or knockdown (Fig 5F).

The Arabidopsis root system is determined by the production of lateral roots, which originate from the growing root, and adventitious roots (ARs), which are formed from non-root organs. WOX11 is a crucial trigger of AR formation (Liu *et al*, 2014; Sheng *et al*, 2017). In standard laboratory conditions, WOX11 does not contribute to LR formation. However, when plants are grown on soil or upon wounding, the primary root can produce both WOX11-mediated roots and non-WOX11-mediated roots (Sheng *et al*, 2017). Interestingly WOX11-mediated and non-WOX11-mediated root initiation converges on the activation of LBD16 (Sheng *et al*, 2017). This led us to examine whether *WOX11* is involved in LBD16 regulation upon TOR knockdown. We observed that *WOX11* transcription increases in the *UB10pro>>amiR-TOR* mutant or upon AZD treatment (Fig 6A; Appendix Fig S12). To know in which tissue *WOX11* is expressed upon *TOR* knockdown, we crossed a *WOX11pro::GUS* line to *UB10pro>>amiR-TOR*. In control conditions, and as previously reported by Sheng *et al*, the *WOX11pro::GUS* signal was undetectable during LR formation; more specifically, WOX11 expression was absent in xylem-pole pericycle cells. Upon TOR knockdown, we observed the *WOX11 pro::GUS* signal in the pericycle (Fig 6B). Together, these data show that TOR inhibition or knockdown (Appendix Fig S12) promotes *WOX11* expression. In these conditions, *LBD16* transcription is promoted independently of ARF7/19 (Sheng *et al*, 2017; Fig 6C). Through its control of LBD16 translation, TOR would also control the WOX11-dependent root branching. To test this hypothesis, we cut the root of the *arf7/arf19* double mutant to induce the formation of only WOX11-dependent side roots (Sheng *et al*, 2017). On 1/2MS medium 6 days after excision, we observed the expected formation of roots near the wounded region (Fig 6D and F). On 1/2MS medium containing AZD, no roots were formed near the cut side (Fig 6E and G), indicating that TOR activity is also required for the non-canonical, WOX11-dependent primary root branching (Fig 6H). WOX11-mediated root initiation is a hallmark of root formation from autotrophic tissues (hypocotyl, leaves) that can be coopted for noncanonical primary root branching upon stress (Sheng *et al*, 2017). By inhibiting *WOX11* expression, TOR prevents the activation of this fail-safe branching mechanism in sink tissue (Fig 6H). In source tissue such as the hypocotyl, reduction of TOR abundance (amiR-TOR) or its activity (*lst8* mutant) does not prevent AR formation induced by WOX11 up-regulation and may even promote it (Fig EV1). The role of TOR in AR formation has been reported in Arabidopsis (Deng *et al*, 2017). However, inhibition of TOR activity reduced AR formation, a difference from what we observed. The difference in response may arise from the conditions used. Deng *et al* scored AR formation in dark-grown hypocotyl where the root was removed, while in our case, plants were grown in light with intact roots. These differences

© 2023 The Authors

may hint at the existence of complex regulation of TOR roles in autotrophic tissues in response to different physiological status. How TOR levels modulate the expression of WOX11 and how, in the hypocotyl, TOR regulation of LBD16 is alleviated remain to be elucidated.

These results shed light on the metabolic control of root branching. They reveal the central role TOR plays in an organ entirely dependent on the supply of carbohydrates from the source tissues in matching the availability of resources to the decision to form a new organ.

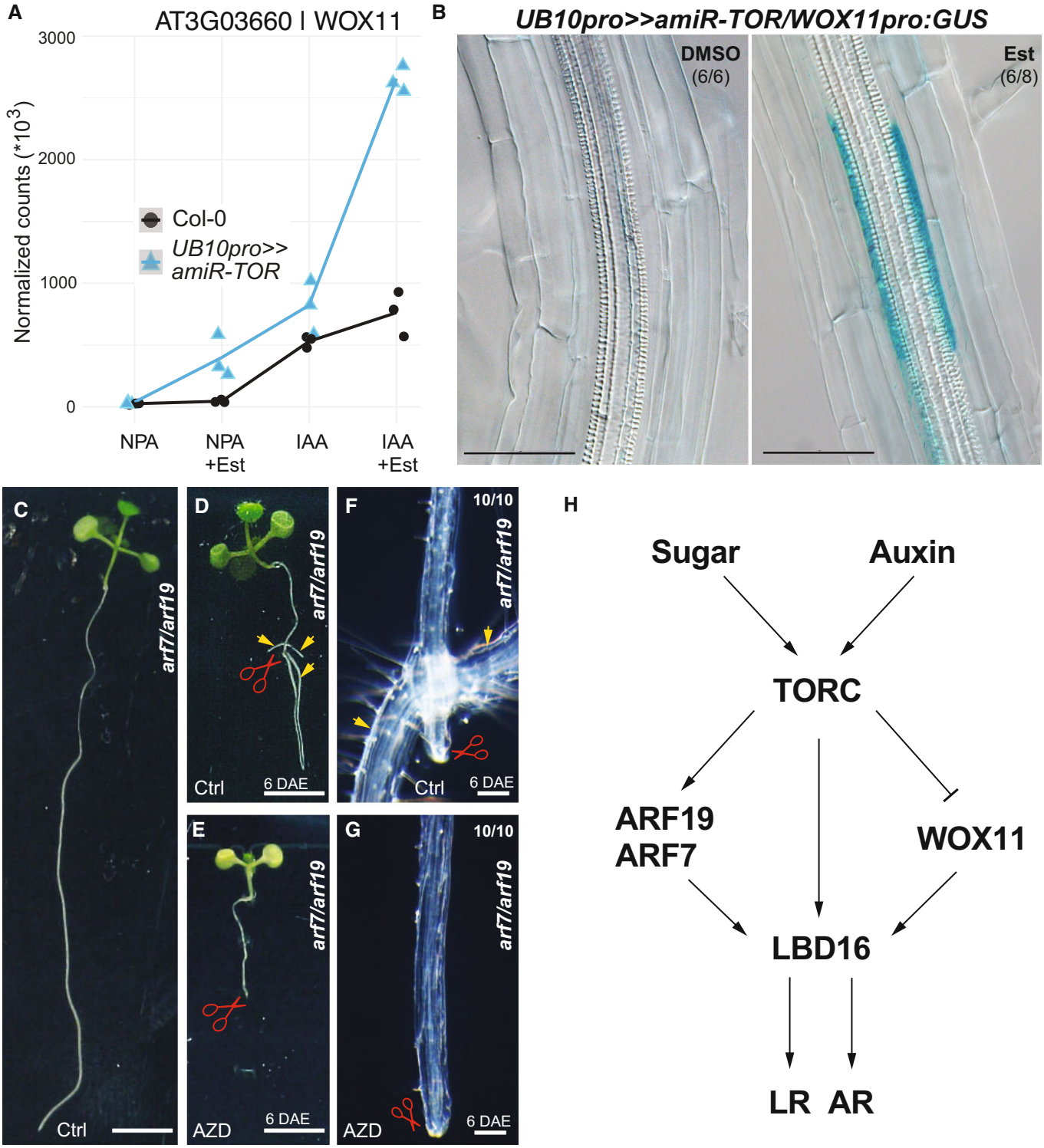

Figure 6.

© 2023 The Authors

Figure 6. TOR is required for aARF7/ARF19 independent formation of adventitious roots via WOX11.

A Abundance of *WOX11* transcripts in RNAseq samples. mRNA accumulation in response to auxin is elevated when TOR is knocked down. $n = 3$ biological replicates.
B Distribution of GUS-staining in *UB10pro>>amiR-TOR/WOX11pro::GUS* seedlings 6 days after transfer to 10 μM Est. The proportion of root bends with the depicted phenotype is indicated.
C The *arf7/arf19* mutant shows defective LR initiation.
D Formation of roots (arrows) close to the wound site of *arf7/arf19* primary roots 6 days after excision (DAE).
E Blocking TOR-activity via exposure to 10 μM AZD8055 (AZD) resulted in the loss of rooting capability on the wound site of *arf7/arf19* primary roots at 6 DAE. Scale bars = 3 mm.
F, G Close-ups indicate root formation location or absence of root formation on ctrl media and AZD-containing media, respectively, in *arf7/arf19* primary roots at 6 DAE. The proportion of root wound sites with the depicted phenotype is indicated. Scale bars = 100 μm.
H Model for TOR dependency of root branching in *Arabidopsis*.

Source data are available online for this figure.

Materials and Methods

Reagents and Tools table

Reagent/resource	Reference or source	Identifier or catalog number
Experimental models		
DR5:GUS	Benková *et al* (2003)	
arf7/arf19	Okushima *et al* (2007)	
LBD16-SRDX	Goh *et al* (2012)	
slr	Fukaki *et al* (2002)	
pGATA23::shy2-2-GR and *pGATA23::slr1-GR*	Ramakrishna *et al* (2019)	
TOR-oe	Deprost *et al* (2007)	G548
raptor1b-1	Salem *et al* (2017)	SALK_101990
lst8	Moreau *et al* (2012)	
35Spro::GFP-RPL18	Mustroph *et al* (2009)	
pARF19-5′UTR::mVenus	Truskina *et al* (2021)	
gLBD16-GUS	Sheng *et al* (2017)	
p35S:HF-GFP- RPL18	Mustroph *et al* (2009)	N69096
pWOX11::GUS	Liu *et al* (2014)	
Recombinant DNA		
pUB10:S6K1-3xHA	This study	
UB10pro>>amiR-TOR	This study	
XPPpro>>amiR-TOR	This study	
pRAPTOR1B::GUS:eGFP	This study	
pS6K1:gS6K1-CFP	This study	
Antibodies		
Anti-S6K1 (phospho T449)	Abcam	ab207399
Anti-S6K1/2	Agrisera AB	AS12-1855
Oligonucleotides and sequence-based reagents		
PCR primers	This study	Dataset EV2
Chemicals, enzymes and other reagents		
IAA	Sigma-Aldrich	I2886
Naphthylphthalamic acid (NPA)	Sigma-Aldrich	N0640
AZD8055	MedChemExpress	HY-10422
2-Deoxyglucose	Sigma-Aldrich	D9761
ß-estradiol	Sigma-Aldrich	E2758

© 2023 The Authors

Reagents and Tools table (continued)

Reagent/resource	Reference or source	Identifier or catalog number
amyloglucosidase	Roche	ROAMYGL
Ribitol	Sigma-Aldrich	PHR3526
N-Methyl-N-trimethylsilyltrifluoracetamid	Sigma-Aldrich	M7891
SYBR-Green Mix	Thermo Fisher	4,368,577
GFP-Trap®	Chromotek	gtma
TRIzol	Invitrogen	15,596,026
Complete Protease Inhibitor EDTA-free	Roche	04693159001
Software		
R	https://www.r-project.org/	
TargetSearch	Cuadros-Inostroza *et al* (2009)	
DeSeq2	Love *et al* (2014)	
STAR	https://github.com/alexdobin/STAR	v2.5.2
Fiji	Schindelin *et al* (2012)	
Other		
Illumina NexSeq 500	Illumina	
Ribo-Zero Plus rRNA Depletion Kit	Illumina	

Methods and Protocols

Plant material and growth conditions

Plants of *Arabidopsis thaliana* ecotype Colombia (Col-0) were grown under fluorescent illumination (50 μE m^{-2} s^{-1}) in long-day conditions (16-h light/8-h dark) at 22°C. Seeds were surface sterilized (ethanol 70% and SDS 0.1%) and placed on ½ Murashige and Skoog (MS) medium adjusted to pH 5.7 containing 1% agar (Duchefa). Following stratification (4°C in the dark, > 24 h).

Construction of vectors and plant transformation

Unless specified otherwise, the plasmids were generated using the GreenGate modular cloning system (Lampropoulos *et al*, 2013). For *pUB10:S6K1-3xHA*, the following modules were combined in pGGZ003: *UBQ10 promoter* (A), *B-dummy* (B), *S6K1* (AT3G08730, obtained by PCR on Col-0 gDNA; 1,398 bp) (C), *3xHA* (D), *35S terminator* (E) and *p35S:D- alaR:t35S* (F). The ß-Estradiol inducible amiR-TOR line (*UB10pro>>amiR-TOR)* was designed based on (Siligato *et al*, 2016), and two intermediate vectors (pAP039 and pAP043) were combined in pGGZ003. For pAP039 the following modules were combined in pGGM000: *pGGA044 Olex TATA* (A), *B-dummy* (B), TOR amiRNA (TTTATAACAACAAGTTGGCGT, generated in this study, C), *D-dummy* (D), *RBCS* terminator (E) 250 bp HA adapter (G). For pAP043, the following modules were combined in pGGN000: *UBQ10 promoter* (A) *B-dummy* (B), CDS of chimeric *TF XVE* amplified from pLB12 (Brand *et al*, 2006) in two PCRs to domesticate an endogenous Eco31I site. (C), *D-dummy* (D), *UBQ10 terminator* (E) 250 bp HA adapter (G). For *XPPpro>>amiR-TOR* (*pXPP::LhG4:GR/6xOP::amiR-TOR*), the intermediate module pAP097 was built consisting of *HA-adaptor*, *6xOp* (A), *B-dummy* (B), *TORamiRNA* (C), *D-dummy* (D), *UB10* terminator (E) and HygrR (F) in pGGN000, and combined with pSW303 (in pGGM000) consisting of *pXPP* (A), *B-dummy* (B), *LhG4:GR* (C), *D-dummy* (D), *RBCS* terminator (E) FH-adaptor (F). Both modules were combined in pGGZ003 to generate the final vector. For the *pRAPTOR1B::GUS:eGFP* transcriptional fusion, 1,360 bp upstream of the of *RAPTOR1B* (*AT3G08850*) were amplified by PCR, cloned into the pDONR221TM P1P2 by BP reaction (BP clonase, Thermofisher), and sub-cloned into the destination vector pHGWFS7.0 by LR reaction (LR clonase, Thermofisher). The *pS6K1:gS6K1-CFP* is an S6K1 genomic line with a C-terminal CFP clone. It was generated by PCR amplification (DNA KOD Hot-start DNA Polymerase, Novagen), cloned into the pENTRD-TOPO Gateway vector using the manufacturer's protocol, and confirmed by sequencing. This clone was then used as a template to generate AscI-S6K1p::S6K1g(No STOP)-PacI fragments that were then ligated into the promoterless pBa002a vector to generate pBa002a/S6K1p::S6K1g-CFP. The clone was confirmed by sequencing. The primers used for cloning and sequencing are listed in Dataset EV2. Agrobacterium tumefaciens (Agl-0, GV3101 or ABI50) based plant transformation was carried out using the floral dip method (Clough & Bent, 1998). All plant lines examined were homozygous if not indicated otherwise. Homozygosity was determined by antibiotic resistance, and three independent lines were analyzed in the T3 generation.

Pharmacological treatments

For IAA treatments (10 μM), samples were treated for 6 h before sampling. TOR inhibitor AZD8055 (10 μM) was applied for 16 h before inducing LR formation by auxin for an additional 6 h. Similarly, seedlings were transferred for 16 h to 2-Deoxyglucose (20 mM) containing media to block glycolysis before seedlings were treated for an additional 6 h with auxin to induce LR formation. UB10pro>>amiR-TOR was expressed by transferring seedlings to plates containing ß-Estradiol (10 μM) for 24 h.

Synchronous induction of lateral root induction

We used the previously described LR-inducible system (Himanen *et al*, 2002). In brief, dense horizontal lanes of sterilized seeds were

 © 2023 The Authors

placed on sterile nylon membranes (SEFAR, Switzerland) and, 7 days after germination, were transferred to plates with fresh ½ MS medium containing 10 μM NPA (Naphthylphthalamic acid for 24 h before shifting to 10 μM IAA).

Starch quantification

Enzymatic quantification of starch was conducted according to (Smith & Zeeman, 2006) with few modifications. In brief, for each of the four replicates, rosettes of 4–6 individual plants at 15 DAG were snap-frozen in liquid nitrogen, weight, and tissue lyzed before being boiled twice in 90% (v/v) ethanol. The decolored ground tissues were washed with 100% ethanol and once with water. Starch in the insoluble remains was hydrolyzed by adding 200 μl 0.2 M KOH and heating for 1 h at 95°C before neutralizing the solution via the application of 35 μl 1 M acetic acid and boiled for 30 min. Total starch in 50 μl of the resulting solution was then digested into glucose monomers via amyloglucosidase at 37°C overnight and further processed for starch quantification as described in (Smith & Zeeman, 2006).

GC–MS-based metabolite profiling

Profiling of central carbon metabolism intermediates was performed using GC–MS according to metabolite extraction and analysis steps initially as described previously (Roessner *et al*, 2001). Briefly, 15–40 mg of the previously collected frozen root tissues was homogenized by tissue lyzer in liquid nitrogen and mixed with 360 μl ice-cold methanol. 20 μg of Ribitol was added as an internal normalizing standard. After extraction (15 min, 70°C), 200 μl chloroform and 400 μl water were added, and samples were mixed vigorously before centrifugation. 200 μl of the upper methanol–water phase containing polar to semipolar metabolites was collected and dried in a vacuum concentrator. Derivatization followed thereafter, including methoximation of the concentrated residues followed by silylation. To this end, the residues were first re-suspended in a methoxyamine-hydrochloride/pyridine solution to methoxymize the carbonyl groups. Samples were then heated (90 min, 37°C) and subsequently silylated with *N*-methyl-*N*- trimethylsilyltrifloracetamide (37°C, 30 min). GC–MS analysis was performed on a gas chromatograph system equipped with a quadrupole mass spectrometer (GC-MS-QP2010, Shimadzu, Duisburg, Germany). For this, 1 μl of each sample was injected in split mode with a split ratio of 1:100, and the separation of derivatized metabolites was carried out on an RTX-5MS column (Restek Corporation, Bellefonte, PA) using instrumental settings optimized by (Lisec *et al*, 2006).

GC–MS data processing

Raw GC–MS data files were first converted into an ANDI-MS universal file format for spectrum deconvolution and compound identification. Baseline correction, peak identification, retention time (RT) alignment, and library matching with the reference collection of the Golm Metabolome Database (GMD, http://gmd.mpimp-golm.mpg.de/) were obtained using the TargetSearch R package from Bioconductor (Cuadros-Inostroza *et al*, 2009). Kovats retention indices used for library matching were calculated for deconvoluted mass spectra from measurements of an alkane mixture (Sigma-Aldrich, St. Louis, MO). The Shimadzu GCMS solutions software (v2.72) interface was further used for the manual curation of annotation of some metabolites versus authentic standards analyzed under the above-described analytical conditions. CSV output files (shoot and root data sets) from the data processing were exported with peak areas obtained for quantifier ions selected for deconvoluted spectra consistently detected in all analyzed samples. Peak areas (Dataset EV1) were scaled on a sample basis according to the extracted amount of root tissue and relative to the peak area obtained for the ribitol internal standard to correct for putative extraction and analytical performance variations across the different measurements. Finally, peak areas for the abovementioned compounds obtained in solvent/blank samples were subtracted as background signals from biological samples. For hierarchical clustering analysis of normalized relative peak levels, data were *z*-score transformed, and clustering was conducted with Ward's clustering method.

S6K phosphorylation assay

For each sample, dissected and flash-frozen roots of ca. 200 seedlings were used. Proteins were extracted from 40 mg root materials in 200 μl 1× MOPS buffer (0.1 M MOPS, 50 mM NaCl, 5% SDS, 10% glycerol, 4 mM EDTA [pH 7.5], 0.3% ß-mercaptoethanol) supplemented with 1.5% phosphatase inhibitor cocktail 2 (Sigma-Aldrich, St. Louis, MO). After adding extraction buffer, samples were briefly mixed and heated at 95°C for 7 min. Cellular debris was removed by centrifugation (10 min, 14,000 rpm, RT). Protein extracts were supplemented with 5x Laemmli buffer (Bromophenol blue [0.05%], 0.3 M Tris buffer [pH 6.8], 50% glycerol, 0.1 M DTT) and reheated for 5 min to 95°C. 20 μl protein extract was separated on a 12% SDS gel and transferred to a Nitrocellulose membrane (Sigma-Aldrich, St. Louis, MO). Anti-S6K1 (phospho T449) polyclonal antibody (No. ab207399, Abcam, Cambridge, UK) was used to detect S6K phosphorylation. S6K1/2 antibody (AS12-1855, Agrisera AB, Vännäs, Sweden) was used to detect total S6K1, Ponceau-S counterstain for confirmation of equal loading.

Histochemical analysis and microscopy

GUS activity was assayed at 37°C overnight following a modified version of the protocol (Weigel & Glazebrook, 2002): the initial washing with the staining buffer (without X-Gluc) and vacuum steps were omitted. GUS staining was followed by fixation in a 4% HCl and 20% methanol solution (15 min at 65°C), followed by 7% NaOH in 60% ethanol (15 min, room temperature). Seedlings were subsequently cleared in successive ethanol baths for 10 min (40, 20, 10%), followed by a 20 min incubation in 25% glycerol and 5% ethanol. Finally, seedlings are mounted in 50% glycerol for imaging with DIC microscopy using an Axio Imager. M1 (Carl 478 Zeiss, Oberkochen, Germany) with a 20× objective. For starch staining, seedlings were collected in the morning of the indicated DAG, fixed and cleared as described above, then stained for 30 min with 2 ml of Lugol's Iodine solution according to (Caspar *et al*, 1985) and immediately scanned using a RICOH IM C3000 system (https://www.ricoh-europe.com/). Calcofluor White counterstaining was performed with seedlings fixed for 30 min in 4% PFA in 1× PBS (RT), as described (Ursache *et al*, 2018). Root bend sections were cleared with ClearSee (Kurihara *et al*, 2015)for 1 day and imaged on a Leica SP8 confocal microscope with a 40×, NA = 1.3 oil immersion objective. Calcofluor White fluorescence was detected using the 405 nm excitation laser line and an emission range of 425–475 nm. mVENUS was detected using the 488 nm excitation laser line and an emission range of 500–550 nm.

© 2023 The Authors

Lateral root quantification

Seedlings were grown for 14 days on square dishes placed upright under a long-day light regime as described above. Plates were subsequently scanned using a RICOH IM C3000 system (https://www.ricoh-europe.com/), and primary root length was measured with fiji. Using a stereomicroscope (SteREO Discovery.V12, Zeiss, Jena), all emerged LR on each seedling were counted, and subsequently, the density of LR per cm of primary root was calculated.

Roots resection

Root cutting in the arf7/arf19 mutant was performed as described previously (Sheng *et al*, 2017) with the following modification, plants were cut at 8 DAG.

RNA-seq analysis

Samples (Col-0 or inducible *UB10pro>>amiR-TOR* line) were prepared for harvesting using the synchronous induction of lateral root procedure. All samples were pre-treated with 10 μM NPA for 24 h, then shifted to plates containing 10 μM NPA and 10 μM Estradiol or DMSO control for an additional 24 h before being shifted to either 10 μM IAA + 10 μM Estradiol or DMSO for LR induction or maintained on the same plates. Root tissue was harvested after 6 h. All sampling points were performed in triplicate. About 200 segments of the lower two-thirds seedling roots were pooled for each sample. The total RNA of the 24 samples (2 genotypes × 4 treatments × 3 replicates) was extracted with the Universal RNA purification kit (EURx). Illumina NextSeq libraries were prepared from 2 μg of total RNA, and sequencing was performed on NextSeq 500 flow cells (12 samples per cell). Reads were mapped onto the *Arabidopsis thaliana* genome (TAIR10), and the number of reads per transcript was computed using STAR (version 2.5.2b). All the subsequent analysis was done with R (www.r-project.org/) using the DESeq2 package (Love *et al*, 2014). Differentially expressed genes were identified using a grouping variable that combines the Treatment (NPA, NPA_Est, IAA, IAA_ESt) and Genotype (col-0, *UB10pro>>amiR-TOR*) variables at log2 fold change > 1 and false discovery rate < 0.05. The procedure was inspired by workflow. The 1,141 genes induced by IAA were defined as the differentially expressed genes (NPA vs. IAA) common that were insensitive to the effect of Estradiol in col-0. The RNASeq data have been deposited to GEO (GSE199202) as part of the SuperSeries GSE199211.

RT–qPCR

Seedlings were pretreated at 7 DAG for 16 h either with 10 μM AZD8055 or DMSO control media before being transferred to DMSO, 10 μM IAA, 10 μM AZD8055 or 10 μM AZD8055 + 10 μM IAA. Root tissues of ca. 200 seedlings were then dissected after 6 h. All samplings were performed in quintuplicate or quadruplicate. Total RNA was extracted with the RNeasy Plant Mini Kit (Qiagen), and 2 μg RNA was reverse transcribed with RevertAid First Strand cDNA Synthesis Kit (Thermo Fisher). Quantitative RT–PCR (RT–qPCR) was performed using gene-specific primers (see Dataset EV2) in a total volume of 20 μl Absolute qPCR SYBR-Green Mix (Thermo Fisher) on a qTOWER^3 (Analytik Jena) apparatus according to the manufacturer's instructions.

TRAP-Seq

The TRAP-seq experiment was conducted according to Thellmann *et al* (2020). In brief, seedlings ubiquitously expressing a GFP-tagged RPL18 ribosomal protein (*p35S:HF-GFP- RPL18*, N69096; Mustroph *et al*, 2009) were pretreated at 7 DAG for 16 h either with 10 μM AZD8055 or DMSO control media before being transferred to DMSO, 10 μM IAA, 10 μM AZD8055 or 10 μM AZD8055 + 10 μM IAA. Root tissues were then dissected after 6 h. All samplings were performed in triplicate. For each sample, about 1,500 segments of the lower two-thirds of the seedling roots were pooled, flash-frozen in liquid nitrogen, and later homogenized with a polysome-extraction buffer (Thellmann *et al*, 2020). The suspension was centrifuged for 15 min (16,000 *g*, 4°C). An aliquot of the homogenate was used for Bulk-RNA- extraction by TRIzol reagent (Invitrogen). The remaining supernatant was incubated with GFP-Trap® Magnetic Agarose beads (Chromotek, Munich, Germany). Ribosomal bound RNA was obtained by immunoprecipitation with magnetic anti-GFP beads following the manufacturer's instructions and subsequently purified by TRIzol reagent (Invitrogen). Illumina NextSeq libraries were prepared from 2 μg of total RNA (bulk) or 100 ng (Ribosome bound) after depleting the rRNA via Ribo-Zero Plus rRNA Depletion Kit (Illumina) and sequencing performed on NextSeq 500 flow cells (12 samples per cell). Reads were mapped onto the Arabidopsis thaliana genome (TAIR10), and the number of reads per transcript was computed using STAR (version 2.5.2b). All the subsequent analysis was done with R (www.r-project.org/) using the DESeq2 package (Love *et al*, 2014). For each assay type (Bulk and TRAP), the variance was stabilized by a -log transform, and z-score were derived for all transcripts genome-wide. The log10 ratio of TRAP to Bulk signal was then computed for all transcripts. The auxin-responsive genes used for k-means clustering based on the ratio of TRAP to Bulk signal were identified in the Bulk set comparing DMSO to IAA treatment ($|\log2FC| > 1$, FDR < 0.05). The TRAP-Seq and Bulk RNA seq data have been deposited to GEO (GSE199203) as part of the SuperSeries GSE199211.

Polysome profile analysis

Root samples were frozen and ground in liquid nitrogen. The powder was resuspended in Polysome extraction buffer (100 mM HEPES-KOH pH 8.0, 150 mM KCl, 25 mM Mg(OAc)2, 25 mM EGTA pH 8.0, 0.5% NP-40, 250 mM sucrose, 5 mM dithiothreitol [DTT], Complete Protease Inhibitor EDTA-free [Roche]), and the final lysate was cleared by high-speed centrifugation for 15 min at 4°C. The equivalent of 100 a.u. (A260; measured on Nanodrop) was layered on top of the 15–45% (w/v) sucrose density gradients and then centrifuged at 29,000 rpm in a SW60-Ti rotor for 3 h at 4°C. The polysome profiles were generated by continuous absorbance measurement at 260 nm using a Gradient Fractionation System (Biocomp Instruments), eight fractions were collected, and total RNA from individual fractions was extracted with Tri-Reagent (Trizol) and reverse transcribed with High-Capacity cDNA Reverse Transcription Kit (Applied Biosystem). Quantitative RT–PCR (RT–qPCR) was performed using gene-specific primers (see File S2) in a total volume of 10 μl SYBR Green Master mix (Roche) on a LightCycler LC480 apparatus (Roche) according to the manufacturer's instructions.

Statistical analysis

Plants were randomly assigned to groups and treatments during sowing. Samples size was not determined in advance; the largest possible number of plants per group was analyzed. No blinding measure was installed. Statistical analyses were performed with R.

 © 2023 The Authors

Normality was tested using the Shapiro–Wilk test; if not met, a non-parametric test was used. Levene's test tested the assumption on equality of variance; if not met, the assumption was relaxed in the test. The methods and *P*-values are summarized in the figure legends. Data were plotted using R and Microsoft Excel.

Data availability

The datasets produced in this study are available in the following databases: RNA-Seq data: Gene Expression Omnibus GSE199211 (https://www.ncbi.nlm.nih.gov/geo/query/acc.cgi?acc=GSE199211).

Expanded View for this article is available online.

Acknowledgments
We thank A. Leibfried for critically reading the manuscript, M. Burow (DynaMo Center, Dept. of Plant and Environmental Sciences, University of Copenhagen, Denmark) for *TOR-oe* seeds, S. Savaldi-Goldstein (Faculty of Biology, Technion Haifa, Israel), for the *p35S:HF- GFP-RPL18* line, A. Bishopp (University of Nottingham, UK) for the *pARF19-5′UTR::mVenus* line, Christian Meyer for sending the *lst8* seeds—twice (INRA, Institute Jean-Pierre Bourgin) and Lin Xu (Institute of Plant Physiology and Ecology, Shanghai, PRC) for the *gLBD16-GUS* line and Lin Xu for providing the *WOX11pro:GUS* line. The authors gratefully acknowledge the data storage service SDS@hd supported by the Ministry of Science, Research and the Arts Baden-Württemberg (MWK), the COS Metabolomics Core Technology Platform for GC/MS instrument access, the Cluster of Excellence Cellular Networks of the University of Heidelberg (CellNetworks) through grant EcTOP6 "Metabolism and Development" and the German Research Foundation (DFG) through grants INST 35/1314-1 FUGG, INST 35/1503-1 FUGG and FOR2581. Open Access funding enabled and organized by ProjektDEAL. Open Access funding enabled and organized by Projekt DEAL.

Author contributions
Michael Stitz: Conceptualization; resources; data curation; formal analysis; validation; investigation; visualization; methodology; writing – original draft; writing – review and editing. **David Kuster:** Data curation; formal analysis; investigation; writing – review and editing. **Maximillian Reinert:** Data curation; investigation. **Mikhail Schepetilnikov:** Data curation; formal analysis; investigation; visualization. **Béatrice Berthet:** Data curation; formal analysis; investigation. **Jazmin Reyes-Hernández:** Data curation; investigation. **Denis Janocha:** Resources; writing – review and editing. **Anthony Artins:** Resources. **Marc Boix:** Resources. **Rossana Henriques:** Resources. **Anne Pfeiffer:** Resources. **Jan Lohmann:** Resources. **Emmanuel Gaquerel:** Conceptualization; data curation; formal analysis; supervision; funding acquisition; visualization; methodology; writing – original draft; project administration; writing – review and editing. **Alexis Maizel:** Conceptualization; formal analysis; supervision; funding acquisition; visualization; methodology; writing – original draft; project administration; writing – review and editing.

Disclosure and competing interests statement
The authors declare that they have no conflict of interest.

References

Andersen TG, Naseer S, Ursache R, Wybouw B, Smet W, De Rybel B, Vermeer JEM, Geldner N (2018) Diffusible repression of cytokinin signalling produces endodermal symmetry and passage cells. *Nature* 555: 529 – 533

Arrivault S, Guenther M, Ivakov A, Feil R, Vosloh D, van Dongen JT, Sulpice R, Stitt M (2009) Use of reverse-phase liquid chromatography, linked to tandem mass spectrometry, to profile the Calvin cycle and other metabolic intermediates in *Arabidopsis* rosettes at different carbon dioxide concentrations. *Plant J* 59: 826 – 839

Atkinson JA, Rasmussen A, Traini R, Voß U, Sturrock C, Mooney SJ, Wells DM, Bennett MJ (2014) Branching out in roots: uncovering form, function, and regulation. *Plant Physiol* 166: 538 – 550

Bellini C, Pacurar DI, Perrone I (2014) Adventitious roots and lateral roots: similarities and differences. *Annu Rev Plant Biol* 65: 639 – 666

Benková E, Michniewicz M, Sauer M, Teichmann T, Seifertová D, Jürgens G, Friml J (2003) Local, efflux-dependent auxin gradients as a common module for plant organ formation. *Cell* 115: 591 – 602

Blázquez MA, Nelson DC, Weijers D (2020) Evolution of plant hormone response pathways. *Annu Rev Plant Biol* 71: 327 – 353

Brand L, Hörler M, Nüesch E, Vassalli S, Barrell P, Yang W, Jefferson RA, Grossniklaus U, Curtis MD (2006) A versatile and reliable two-component system for tissue-specific gene induction in *Arabidopsis*. *Plant Physiol* 141: 1194 – 1204

Caldana C, Li Y, Leisse A, Zhang Y, Bartholomaeus L, Fernie AR, Willmitzer L, Giavalisco P (2013) Systemic analysis of inducible target of rapamycin mutants reveal a general metabolic switch controlling growth in *Arabidopsis thaliana*. *Plant J* 73: 897 – 909

Cao P, Kim S-J, Xing A, Schenck CA, Liu L, Jiang N, Wang J, Last RL, Brandizzi F (2019) Homeostasis of branched-chain amino acids is critical for the activity of TOR signaling in *Arabidopsis*. *Elife* 8: e50747

Caspar T, Huber SC, Somerville C (1985) Alterations in growth, photosynthesis, and respiration in a starchless mutant of *Arabidopsis thaliana* (L.) deficient in chloroplast phosphoglucomutase activity. *Plant Physiol* 79: 11 – 17

Clough SJ, Bent AF (1998) Floral dip: a simplified method for agrobacterium-mediated transformation of *Arabidopsis thaliana*. *Plant J* 16: 735 – 743

Crookshanks M, Taylor G, Dolan L (1998) A model system to study the effects of elevated CO2 on the developmental physiology of roots: the use of *Arabidopsis thaliana*. *J Exp Bot* 49: 593 – 597

Cuadros-Inostroza A, Caldana C, Redestig H, Kusano M, Lisec J, Peña-Cortés H, Willmitzer L, Hannah MA (2009) TargetSearch – a Bioconductor package for the efficient preprocessing of GC-MS metabolite profiling data. *BMC Bioinformatics* 10: 428

De Rybel B, Vassileva V, Parizot B, Demeulenaere M, Grunewald W, Audenaert D, Van Campenhout J, Overvoorde P, Jansen L, Vanneste S *et al* (2010) A novel aux/IAA28 signaling cascade activates GATA23-dependent specification of lateral root founder cell identity. *Curr Biol* 20: 1697 – 1706

Dembinsky D, Woll K, Saleem M, Liu Y, Fu Y, Borsuk LA, Lamkemeyer T, Fladerer C, Madlung J, Barbazuk B *et al* (2007) Transcriptomic and proteomic analyses of pericycle cells of the maize primary root. *Plant Physiol* 145: 575 – 588

Deng K, Dong P, Wang W, Feng L, Xiong F, Wang K, Zhang S, Feng S, Wang B, Zhang J *et al* (2017) The TOR pathway is involved in adventitious root formation in *Arabidopsis* and potato. *Front Plant Sci* 8: 793 – 718

Deprost D, Yao L, Sormani R, Moreau M, Leterreux G, Nicolaï M, Bedu M, Robaglia C, Meyer C (2007) The *Arabidopsis* TOR kinase links plant growth, yield, stress resistance and mRNA translation. *EMBO Rep* 8: 864 – 870

Dobrenel T, Caldana C, Hanson J, Robaglia C, Vincentz M, Veit B, Meyer C (2016) TOR signaling and nutrient sensing. *Annu Rev Plant Biol* 67: 261 – 285

Dubrovsky JG, Sauer M, Napsucialy-Mendivil S, Ivanchenko MG, Friml J, Shishkova S, Celenza J, Benkova E (2008) Auxin acts as a local

© 2023 The Authors

morphogenetic trigger to specify lateral root founder cells. *Proc Natl Acad Sci USA* 105: 8790 – 8794

Fukaki H, Tameda S, Masuda H, Tasaka M (2002) Lateral root formation is blocked by a gain-of-function mutation in the SOLITARY-ROOT/IAA14 gene of *Arabidopsis*. *Plant J* 29: 153 – 168

Ge Y, Fang X, Liu W, Sheng L, Xu L (2019) Adventitious lateral rooting: the plasticity of root system architecture. *Physiol Plant* 165: 39 – 43

Goh T, Joi S, Mimura T, Fukaki H (2012) The establishment of asymmetry in *Arabidopsis* lateral root founder cells is regulated by LBD16/ASL18 and related LBD/ASL proteins. *Development* 139: 883 – 893

Graf A, Schlereth A, Stitt M, Smith AM (2010) Circadian control of carbohydrate availability for growth in *Arabidopsis* plants at night. *Proc Natl Acad Sci USA* 107: 9458 – 9463

Gupta A, Singh M, Laxmi A (2015) Interaction between glucose and brassinosteroid during the regulation of lateral root development in *Arabidopsis*. *Plant Physiol* 168: 307 – 320

Himanen K, Boucheron E, Vanneste S, de Almeida EJ, Inzé D, Beeckman T (2002) Auxin-mediated cell cycle activation during early lateral root initiation. *Plant Cell* 14: 2339 – 2351

Kircher S, Schopfer P (2012) Photosynthetic sucrose acts as cotyledon-derived long-distance signal to control root growth during early seedling development in *Arabidopsis*. *Proc Natl Acad Sci USA* 109: 11217 – 11221

Kurihara D, Mizuta Y, Sato Y, Higashiyama T (2015) ClearSee: a rapid optical clearing reagent for whole-plant fluorescence imaging. *Development* 142: 4168 – 4179

Lampropoulos A, Sutikovic Z, Wenzl C, Maegele I, Lohmann JU, Forner J (2013) GreenGate – a novel, versatile, and efficient cloning system for plant transgenesis. *PLoS One* 8: e83043

Lavenus J, Goh T, Roberts I, Guyomarc'h S, Lucas M, De Smet I, Fukaki H, Beeckman T, Bennett M, Laplaze L (2013) Lateral root development in *Arabidopsis*: fifty shades of auxin. *Trends Plant Sci* 18: 450 – 458

Lavenus J, Goh T, Guyomarc'h S, Hill K, Lucas M, Voß U, Kenobi K, Wilson MH, Farcot E, Hagen G *et al* (2015) Inference of the *Arabidopsis* lateral root gene regulatory network suggests a bifurcation mechanism that defines primordia flanking and central zones. *Plant Cell* 27: 1368 – 1388

Li X, Cai W, Liu Y, Li H, Fu L, Liu Z, Xu L, Liu H, Xu T, Xiong Y (2017) Differential TOR activation and cell proliferation in *Arabidopsis* root and shoot apexes. *Proc Natl Acad Sci USA* 114: 201618782 – 201618786

Li J, Wang B, Zhu X, Li R, Fu J, Cui H (2020) Novel regulators of sugar-mediated lateral root development in *Arabidopsis thaliana*. *Genes* 11: 1257

Lisec J, Schauer N, Kopka J, Willmitzer L, Fernie AR (2006) Gas chromatography mass spectrometry-based metabolite profiling in plants. *Nat Protoc* 1: 387 – 396

Liu J, Sheng L, Xu Y, Li J, Yang Z, Huang H, Xu L (2014) WOX11 and 12 are involved in the first-step cell fate transition during de novo root organogenesis in *Arabidopsis*. *Plant Cell* 26: 1081 – 1093

Love MI, Huber W, Anders S (2014) Moderated estimation of fold change and dispersion for RNA-seq data with DESeq2. *Genome Biol* 15: 550

Lucas M, Kenobi K, von Wangenheim D, VOβ U, Swarup K, De Smet I, Van Damme D, Lawrence T, Péret B, Moscardi E *et al* (2013) Lateral root morphogenesis is dependent on the mechanical properties of the overlaying tissues. *Proc Natl Acad Sci USA* 110: 5229 – 5234

Malamy JE, Benfey PN (1997) Organization and cell differentiation in lateral roots of *Arabidopsis thaliana*. *Development* 124: 33 – 44

Menand B, Desnos T, Nussaume L, Berger F, Bouchez D, Meyer C, Robaglia C (2002) Expression and disruption of the Arabidopsis TOR (target of rapamycin) gene. *Proc Natl Acad Sci USA* 99: 6422 – 6427

Montané M-H, Menand B (2013) ATP-competitive mTOR kinase inhibitors delay plant growth by triggering early differentiation of meristematic cells but no developmental patterning change. *J Exp Bot* 64: 4361 – 4374

Moreau M, Azzopardi M, Clément G, Dobrenel T, Marchive C, Renne C, Martin-Magniette M-L, Taconnat L, Renou J-P, Robaglia C *et al* (2012) Mutations in the *Arabidopsis* homolog of LST8/GβL, a partner of the target of rapamycin kinase, impair plant growth, flowering, and metabolic adaptation to long days. *Plant Cell* 24: 463 – 481

Muralidhara P, Weiste C, Collani S, Krischke M, Kreisz P, Draken J, Feil R, Mair A, Teige M, Müller MJ *et al* (2021) Perturbations in plant energy homeostasis prime lateral root initiation via SnRK1-bZIP63-ARF19 signaling. *Proc Natl Acad Sci USA* 118: e2106961118

Mustroph A, Zanetti ME, Jang CJH, Holtan HE, Repetti PP, Galbraith DW, Girke T, Bailey-Serres J (2009) Profiling translatomes of discrete cell populations resolves altered cellular priorities during hypoxia in *Arabidopsis*. *Proc Natl Acad Sci USA* 106: 18843 – 18848

Okushima Y, Fukaki H, Onoda M, Theologis A, Tasaka M (2007) ARF7 and ARF19 regulate lateral root formation via direct activation of LBD/ASL genes in *Arabidopsis*. *Plant Cell* 19: 118 – 130

Parizot B, Laplaze L, Ricaud L, Boucheron-Dubuisson E, Bayle V, Bonke M, De Smet I, Poethig SR, Helariutta Y, Haseloff J *et al* (2008) Diarch symmetry of the vascular bundle in *Arabidopsis* root encompasses the pericycle and is reflected in distich lateral root initiation. *Plant Physiol* 146: 140 – 148

Pfeiffer A, Janocha D, Dong Y, Medzihradszky A, Schöne S, Daum G, Suzaki T, Forner J, Langenecker T, Rempel E *et al* (2016) Integration of light and metabolic signals for stem cell activation at the shoot apical meristem. *Elife* 5: e17023

Ramakrishna P, Ruiz Duarte P, Rance GA, Schubert M, Vordermaier V, Vu LD, Murphy E, Vilches Barro A, Swarup K, Moirangthem K *et al* (2019) EXPANSIN A1-mediated radial swelling of pericycle cells positions anticlinal cell divisions during lateral root initiation. *Proc Natl Acad Sci USA* 116: 8597 – 8602

Riegler S, Servi L, Scarpin MR, Godoy Herz MA, Kubaczka MG, Venhuizen P, Meyer C, Brunkard JO, Kalyna M, Barta A *et al* (2021) Light regulates alternative splicing outcomes via the TOR kinase pathway. *Cell Rep* 36: 109676

Roessner U, Luedemann A, Brust D, Fiehn O, Linke T, Willmitzer L, Fernie A (2001) Metabolic profiling allows comprehensive phenotyping of genetically or environmentally modified plant systems. *Plant Cell* 13: 11 – 29

Sairanen I, Novák O, Pěnčík A, Ikeda Y, Jones B, Sandberg G, Ljung K (2012) Soluble carbohydrates regulate auxin biosynthesis via PIF proteins in *Arabidopsis*. *Plant Cell* 24: 4907 – 4916

Salem MA, Li Y, Wiszniewski A, Giavalisco P (2017) Regulatory-associated protein of TOR (RAPTOR) alters the hormonal and metabolic composition of *Arabidopsis* seeds, controlling seed morphology, viability and germination potential. *Plant J* 92: 525 – 545

Santos Teixeira JA, Ten Tusscher KH (2019) The systems biology of lateral root formation: connecting the dots. *Mol Plant* 12: 784 – 803

Scarpin MR, Leiboff S, Brunkard JO (2020) Parallel global profiling of plant TOR dynamics reveals a conserved role for LARP1 in translation. *Elife* 9: e58795

Schepetilnikov M, Dimitrova M, Mancera-Martínez E, Geldreich A, Keller M, Ryabova LA (2013) TOR and S6K1 promote translation reinitiation of uORF-containing mRNAs via phosphorylation of eIF3h. *EMBO J* 32: 1087 – 1102

Schepetilnikov M, Makarian J, Srour O, Geldreich A, Yang Z, Chicher J, Hammann P, Ryabova LA (2017) GTPase ROP2 binds and promotes activation of target of rapamycin, TOR, in response to auxin. *EMBO J* 36: 886 – 903

 © 2023 The Authors

Schindelin J, Arganda-Carreras I, Frise E, Kaynig V, Longair M, Pietzsch T, Preibisch S, Rueden C, Saalfeld S, Schmid B *et al* (2012) Fiji: an open-source platform for biological-image analysis. *Nat Methods* 9: 676 – 682

Schütz LM, Louveaux M, Vilches Barro A, Bouziri S, Cerrone L, Wolny A, Kreshuk A, Hamprecht FA, Maizel A (2021) Integration of cell growth and asymmetric division during lateral root initiation in *Arabidopsis thaliana*. *Plant Cell Physiol* 62: 1269 – 1279

Sharma M, Sharma M, Jamsheer KM, Laxmi A (2022) Jasmonic acid coordinates with light, glucose and auxin signalling in regulating branching angle of Arabidopsis lateral roots. *Plant Cell Environ* 45: 1554 – 1572

Sheng L, Hu X, Du Y, Zhang G, Huang H, Scheres B, Xu L (2017) Non-canonical WOX11-mediated root branching contributes to plasticity in *Arabidopsis* root system architecture. *Development* 144: 3126 – 3133

Shi L, Wu Y, Sheen J (2018) TOR signaling in plants: conservation and innovation. *Development* 145: dev160887

Shyh-Chang N, Ng H-H (2017) The metabolic programming of stem cells. *Genes Dev* 31: 336 – 346

Siligato R, Wang X, Yadav SR, Lehesranta S, Ma G, Ursache R, Sevilem I, Zhang J, Gorte M, Prasad K *et al* (2016) MultiSite gateway-compatible cell type-specific gene-inducible system for plants. *Plant Physiol* 170: 627 – 641

Smith AM, Zeeman SC (2006) Quantification of starch in plant tissues. *Nat Protoc* 1: 1342 – 1345

Sulpice R, Pyl E-T, Ishihara H, Trenkamp S, Steinfath M, Witucka-Wall H, Gibon Y, Usadel B, Poree F, Piques MC *et al* (2009) Starch as a major integrator in the regulation of plant growth. *Proc Natl Acad Sci USA* 106: 10348 – 10353

Thellmann M, Andersen TG, Vermeer JE (2020) Translating ribosome affinity purification (TRAP) to investigate *Arabidopsis thaliana* root development at a cell type-specific scale. *J Vis Exp*10.3791/60919

Torres-Martínez HH, Hernández-Herrera P, Corkidi G, Dubrovsky JG (2020) From one cell to many: morphogenetic field of lateral root founder cells in *Arabidopsis thaliana* is built by gradual recruitment. *Proc Natl Acad Sci USA* 117: 20943 – 20949

Truskina J, Han J, Chrysanthou E, Galvan-Ampudia CS, Lainé S, Brunoud G, Macé J, Bellows S, Legrand J, Bågman A-M *et al* (2021) A network of transcriptional repressors modulates auxin responses. *Nature* 589: 116 – 119

Ursache R, Andersen TG, Marhavý P, Geldner N (2018) A protocol for combining fluorescent proteins with histological stains for diverse cell wall components. *Plant J* 93: 399 – 412

Ursache R, De Jesus Vieira Teixeira C, Dénervaud Tendon V, Gully K, De Bellis D, Schmid-Siegert E, Grube Andersen T, Shekhar V, Calderon S, Pradervand S *et al* (2021) GDSL-domain proteins have key roles in suberin polymerization and degradation. *Nat Plants* 7: 353 – 364

Van Leene J, Han C, Gadeyne A, Eeckhout D, Matthijs C, Cannoot B, De Winne N, Persiau G, Van De Slijke E, Van de Cotte B *et al* (2019) Capturing the phosphorylation and protein interaction landscape of the plant TOR kinase. *Nat Plants* 5: 316 – 327

Vanneste S, Rybel BD, Beemster GTS, Ljung K, Smet ID, Van Isterdael G, Naudts M, Iida R, Gruissem W, Tasaka M *et al* (2005) Cell cycle progression in the pericycle is not sufficient for SOLITARY ROOT/IAA14-mediated lateral root initiation in *Arabidopsis thaliana*. *Plant Cell* 17: 3035 – 3050

Vermeer JEM, von Wangenheim D, Barberon M, Lee Y, Stelzer EHK, Maizel A, Geldner N (2014) A spatial accommodation by neighboring cells is required for organ initiation in *Arabidopsis*. *Science* 343: 178 – 183

Vilches Barro A, Stöckle D, Thellmann M, Ruiz-Duarte P, Bald L, Louveaux M, von Born P, Denninger P, Goh T, Fukaki H *et al* (2019) Cytoskeleton dynamics are necessary for early events of lateral root initiation in *Arabidopsis*. *Curr Biol* 29: 2443 – 2454.e5

Vragović K, Sela A, Friedlander-Shani L, Fridman Y, Hacham Y, Holland N, Bartom E, Mockler TC, Savaldi-Goldstein S (2015) Translatome analyses capture of opposing tissue-specific brassinosteroid signals orchestrating root meristem differentiation. *Proc Natl Acad Sci USA* 112: 923 – 928

Weigel D, Glazebrook J (2002) *Arabidopsis: A Laboratory Manual*. New York, NY: CSHL Press

Xiong Y, McCormack M, Li L, Hall Q, Xiang C, Sheen J (2013) Glucose-TOR signalling reprograms the transcriptome and activates meristems. *Nature* 496: 181 – 186

Zhang SH, Lawton MA, Hunter T, Lamb CJ (1994) atpk1, a novel ribosomal protein kinase gene from *Arabidopsis*. I. Isolation, characterization, and expression. *J Biol Chem* 269: 17586 – 17592

License: This is an open access article under the terms of the Creative Commons Attribution-NonCommercial-NoDerivs License, which permits use and distribution in any medium, provided the original work is properly cited, the use is non-commercial and no modifications or adaptations are made.